Improvements of the coupled WRF-Lake model over Lake Nam Co, Central Tibetan Plateau

Yang Wu[1,2] · Anning Huang[1,2] · Lazhu[3] · Xianyu Yang[4] · Bo Qiu[1] · Lijuan Wen[5] · Zhiqi Zhang[1] · Zhipeng Fu[1] · Xueyan Zhu[1] · Xindan Zhang[1] · Shuxin Cai[1] · Yong Tang[1]

Abstract

A series of model sensitivity simulations are carried out to calibrate and improve the Weather Research and Forecasting Model coupled with a one-dimensional lake model (WRF-Lake) based on observations over Lake Nam Co. Using the default lake model parameters, the solution of WRF-Lake exhibits significant biases in both the lake thermodynamics and regional climatology, i.e., higher lake surface temperature (LST), earlier onset of summer thermal stratification, and overestimated near-surface air temperature and precipitation induced by the lake's excessive warming and moistening impacts. The performance of WRF-Lake is improved through adjusting the initial lake temperature profile, the temperature of maximum water density (Tdmax), the surface roughness length, and the light extinction coefficient. Results show that initializing the water temperature with spring observation mitigates the LST overestimation and reduces the timing error of the onset of thermal stratification. By further adjusting Tdmax from 4 °C to the observed value of 3.5 °C, the LST increase from June to mid-July is enhanced and the buildup of thermal stratification is more accurately predicted. Through incorporating the parameterized surface roughness length and decreasing the light extinction coefficient, the model better reproduces the observed daily evolution of LST and vertical lake temperature profile. The calibrated WRF-Lake effectively mitigates the overestimation of over-lake air temperature at 2 m height and precipitation over regions downwind the lake. This suggests that an improved lake scheme within the coupled WRF-Lake is essential for realistically simulating the lake–air interactions and the regional climate over the lake-rich Tibetan Plateau.

1 Introduction

The Tibetan Plateau (hereafter TP), known as the "Asian Water Tower", harbors more than 1400 lakes with an individual surface area above 1 km^2 (Ma et al. 2011; Zhang et al. 2019a, b). The total lake surface area over TP is approximately 47,000 km^2 and accounts for more than 52% of the total lake coverage in China (Jiang and Huang 2004; Song et al. 2013). As the water body is characterized by lower albedo, smaller surface roughness length, larger heat capacity and thermal conductance when compared with the other land types, the exchanges of water and energy at the lake–air interface distinctly differ from those at the land–air interface, causing the spatial heterogeneity of surface thermal conditions over TP (Gerken et al. 2013; Ma et al. 2014; Song et al. 2016). This would further influence the atmospheric circulation, the weather and climate at local and regional scales (Wu et al. 2019; Zhu et al. 2017). In response to the ongoing climate change and anthropogenic forcing, the TP lakes experience variations in terms of water level/areas

✉ Anning Huang
anhuang@nju.edu.cn

1 CMA-NJU Joint Laboratory for Climate Prediction Studies, School of Atmospheric Sciences, Nanjing University, No. 163 Xianlin Avenue, Nanjing 210023, Jiangsu, China

2 Key Laboratory of Mesoscale Severe Weather/MOE and School of Atmospheric Sciences, Nanjing University, Nanjing 210023, China

3 National Tibetan Plateau Data Center, Institute of Tibetan Plateau Research, Chinese Academy of Sciences, Beijing 100101, China

4 Plateau Atmosphere and Environment Key Laboratory of Sichuan Province, School of Atmospheric Sciences, Chengdu University of Information Technology, Chengdu 610225, China

5 Key Laboratory of Land Surface Process and Climate Change in Cold and Arid Regions, Chinese Academy of Sciences, Lanzhou 730000, China

(Jiang et al. 2017; Kleinherebrink et al. 2015; Zhang et al. 2017), aquatic biogeochemistry (Karl et al. 2018; Sahoo et al. 2016), and ice coverage (Lang et al. 2018; Qi et al. 2019). The TP lakes also take significant feedbacks to the climate and environmental changes (Guo et al. 2019; Neckel et al. 2014; Liao et al. 2013; Yan et al. 2018). Hence, it is imperative to have a comprehensive understanding of the lake–air interactions over TP.

Owing to the high terrain and harsh climate conditions over TP, the in-situ lake observations are limited and inconsecutive, far from being adequate for studying the alpine lake–air interactions and the associated climatic effects (Huang et al. 2017; Wang et al. 2009, 2015, 2019; Biermann et al. 2014). As an alternative, the high-resolution weather/climate models with the consideration of lake impacts are able to simulate the lake-induced spatiotemporal heterogeneity of meteorological elements (i.e., precipitation, temperature and turbulent fluxes), to elucidate the involved underlying mechanisms, and to project future lake variations under different climate change scenarios (Hwang et al. 2019; Wang et al. 2017; Wen et al. 2015; Xiao et al. 2018; Zhu et al. 2017). During the recent decades, many one-dimensional (1-D) and three-dimensional (3-D) lake models with different complexities have been developed and improved to study the lake–air interactions. In contrast to the 1-D models, the 3-D models can resolve both the lake hydrodynamics and thermodynamics explicitly, hence can accurately depicting the lake physical characteristics (Huang et al. 2010; Notaro et al. 2013; Xue et al. 2016). However, the two-way coupling of a 3-D lake model with the other components of a regional climate model requires much more computational power due to the high horizontal resolution (around 2 km) and the complicated physical processes (Nyamweya et al. 2016; Pan et al. 2002; Song et al. 2004). Hence, at present, 1-D lake models are commonly used in the coupled regional weather prediction and climate models (Lofgren 1997; Martynov et al. 2012; Mironov et al. 2010; Samuelsson et al. 2010; Williams et al. 2015; Theeuwes et al. 2010; Thiery et al. 2015).

There are many 1-D lake models for lake simulations, including the Mixed-Layer Model (Goyette et al. 2000), the Freshwater Model based on self-similarity theory (Mironov 2008), the eddy-diffusive Hostetler model (Hostetler et al. 1993; Subin et al. 2012), the bulk formulation models (Imberger and Patterson 1981), and the finite-difference models with second-order (k–ε) turbulence closures (Perroud et al. 2009). According to the Lake Model Intercomparison Project (LakeMIP, Stepanenko et al. 2010, 2013), these models involve different degrees of simplifications on lake thermo- and hydro-dynamics, and their performances vary with different model configurations. As the lake–air interactions and the lake mixing regimes are significantly influenced by different lake intrinsic features (i.e., depth,

size and salinity), local orographic conditions and the background atmospheric circulation, it is essential to identify and calibrate the key model parameters or parameterization schemes for the lake processes within the specific research domains (Gu et al. 2015, 2016; Li et al. 2018; Wen et al. 2016; Thiery et al. 2014; Xiao et al. 2016; Zhang et al. 2019a, b). This is of great benefit to improve the representation of the lake–air interaction in climate models for better simulating the LST and regional climate over lake-dominant areas (Balsamo et al. 2012; Mallard et al. 2014; Martynov et al. 2013; Wang et al. 2018;).

In this study, we focused on the performances of the 1-D eddy diffusion lake scheme incorporated with the advanced Weather Research and Forecasting model (WRF-ARW V3.9.1, Skamarock et al. 2008) in simulating the thermal features of Lake Nam Co, which is the second largest brackish lake over the central TP (Fig. 1c), and the lake climatic effect. The default lake scheme originates from the basic concept of the Hostetler lake model and is further improved by Subin et al. (2012) and Gu et al. (2015). At present, the key parameters (i.e., lake temperature profile initialization, Tdmax, surface roughness length, light extinction coefficient and eddy diffusivity) were calibrated by Gu et al. (2015) based on the buoy observations over two plain freshwater lakes (Lake Erie and Lake Superior). However, as most TP lakes are situated in the alpine cold and semi-arid to arid climate zone and are less influenced by the anthropogenic activities, the lake physical properties and the related lake–air interactions show distinctive features from those of the lakes over lowlands and wet regions (Dai et al. 2018a, b; Lazhu et al. 2016; Li et al. 2015; Wang et al. 2017, 2019). This implies that the lake model with default parameter configurations may not appropriately represent the lake–air heat and water exchanges over TP and would cause large biases in simulating the LST or vertical thermal structures of these TP lakes (Huang et al. 2019). Additionally, as the LST and associated turbulent heat fluxes are the important boundary conditions for the atmospheric component, their simulation accuracy directly affects the performances of the lake-resolved climate model and is important for understanding the lake impacts on the regional climate over lake-rich areas (Sharma et al. 2018; Xiao et al. 2018; Xu et al. 2019; Zhang et al. 2016). Hence, based on the observed bathymetry and 1-year in-situ water temperature records of Lake Nam Co, we conduct a series of sensitivity simulations to calibrate the key lake model parameters in describing the lake thermodynamics. The comparisons between the experiments with the default and calibrated lake schemes are used to demonstrate that a better representation of lake–air interactions in the coupled WRF-Lake is indeed beneficial for improving its performance in reproducing the regional climate surrounding Lake Nam Co. Main findings of this work provide valuable information for further improvements and applications
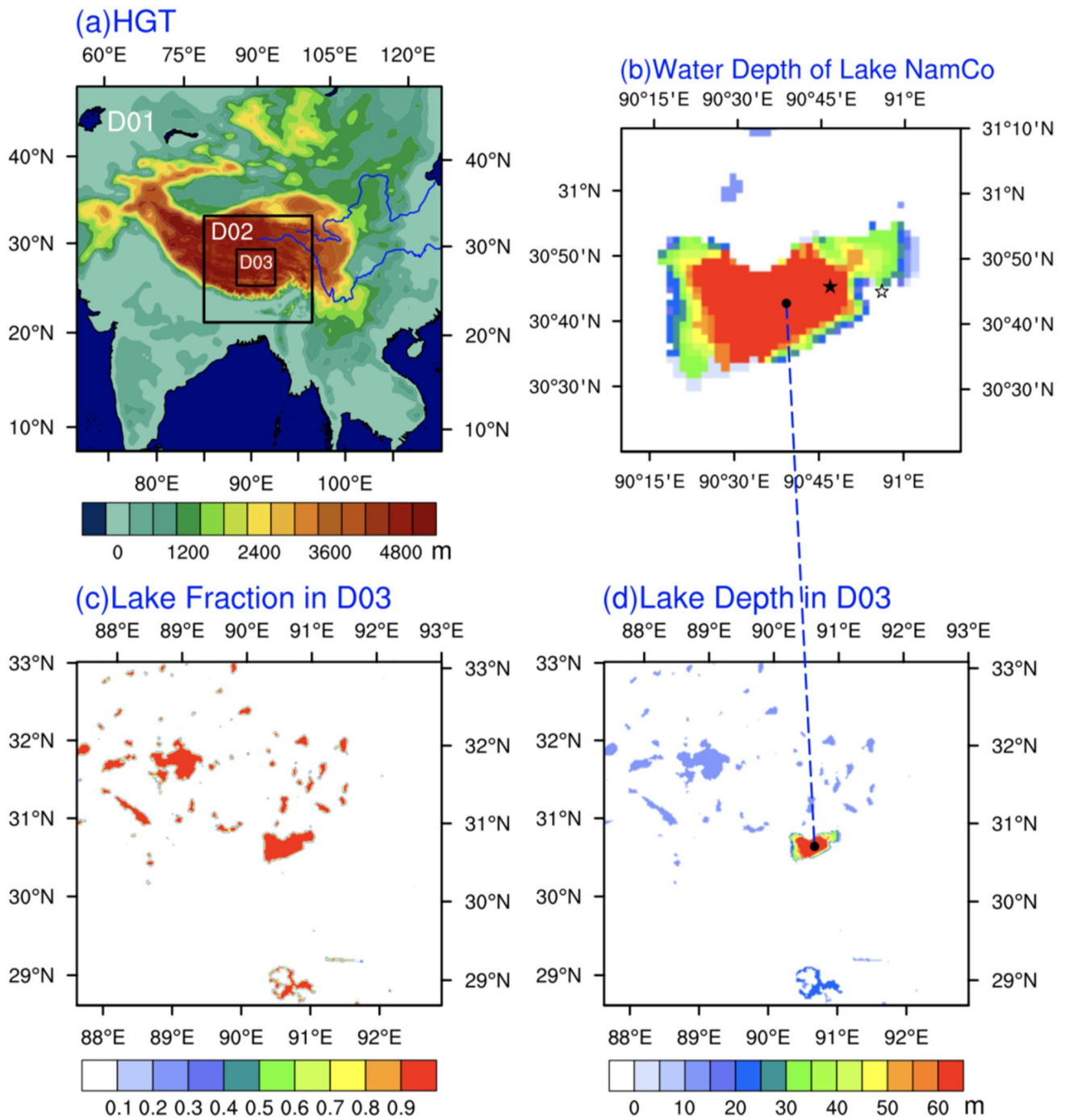
Fig. 1 **a** Geographic locations and terrain height of the three domains; **b** the spatial distributions of the lake depth in Lake Nam Co; **c** the sub-grid lake fraction and **d** depth of lakes in the nested Domain 3. In **a**, the blue curves outline the Yangtze and the Yellow River. The black solid and hollow aster symbol in **b** represent the locations of the lake temperature monitoring station and the automatic weather station at Lake Nam Co, respectively. The color scale of **b** is same as that of **d**

of the coupled lake–air models over alpine and semi-arid to arid lake-rich regions such as TP.

The rest of this paper is organized as follows: The brief descriptions of the coupled WRF-Lake model and experimental designs are firstly introduced in Sect. 2.1. The following

Sects. 2.2 and 2.3 present the lake scheme modifications, and the datasets and methods for evaluation. In Sect. 3, we evaluate the performances of the coupled WRF-Lake with the default and modified lake model parameters in simulating the temporal evolution of LST, the vertical water temperature profile,

and the regional climate. Finally, the conclusion and discussion are presented in Sect. 4.

2 Model description, lake scheme modifications, evaluation data and methodology

2.1 Model description

2.1.1 Overview of the WRF-Lake model

This study evaluates the lake–air coupled WRF V3.9.1 model (Skamarock et al. 2008), whose lake component is a 1-D mass and energy balance lake model from the Community Land Model version 3.5 (Gu et al. 2015; Oleson et al. 2004). The lake model contains up to 5 snow layers on the lake ice, 10 or 25 lake water/ice layers, and 10 soil layers for the bottom sediment. We adopt a 25-layer vertical discretization for the lake column because this setup has been proved to possess advantages in simulating the variations of metalimnion temperature, ice coverage and other lake thermodynamic characteristics (Wang et al. 2018; Xiao et al. 2016). The main physical processes can be divided into two parts: energy exchanges between the lake surface (snow, ice, or water) and the overlying atmosphere and the heat transfer within the lake body (Huang et al. 2019).

Following Subin et al. (2012), the surface heat fluxes are solved using the conditions at the atmospheric reference height as a top boundary condition and the top lake model layer temperature (in the lake body for snow depth < 40 mm and in the snow otherwise) as a bottom boundary condition. The lake surface temperature T_s is solved simultaneously with the friction velocity, surface roughness, and aerodynamic resistances in order to balance the surface energy budget:

$$\beta(1 - \alpha)SW_{\downarrow} + (LW_{\downarrow} - \varepsilon\sigma T_s^4) - SH_{\uparrow} - LH_{\uparrow} = G_{\downarrow}, \qquad (1)$$

where α is the surface albedo for the downward solar radiation $SW_{\downarrow}$(W m^{-2}), $\beta = 0.4$ is the surface absorption rate of the net solar radiation. In the net longwave radiation term $LW_{\downarrow} - \varepsilon\sigma T_s^4$, $\varepsilon = 0.97$ is the lake surface emissivity, $LW_{\downarrow}$ is the incident longwave radiation (W m^{-2}), $\sigma = 5.67 \times 10^{-8}$ Wm^{-2} K^{-4} is the Stefan-Boltzmann constant. $SH_{\uparrow}$ and $LH_{\uparrow}$

are the turbulent fluxes of sensible and latent heat (W m^{-2}), and $G_{\downarrow}$ is the downward heat flux into the lake surface layer (W m^{-2}). For the above variables, positive values mean downward for SW/LW/G, and upward for SH/LH.

The subsurface temperature for the lake column including snow, ice, water, and soil is calculated by a diffusion equation:

$$\frac{\partial T}{\partial t} = \frac{\partial}{\partial z}\left[(k_m + m_d k_e)\frac{\partial T}{\partial z}\right] - \frac{1}{c_w}\frac{d\phi}{dz}, \qquad (2)$$

where T is the water temperature (K) at depth z (m); t is time (s); k_m=1.43×10^{-7} m^2 s^{-1} is the molecular diffusion coefficient; k_e is the wind-driven eddy diffusivity for unfrozen lake (m^{2}s^{-1}); m_d is the mixing factor with a range from 10^2 to 10^5 that is adopted to compensate for the unresolved vertical mixing processes in deep lakes; c_w is the volumetric heat capacity (Jm^{-3} K^{-1}); and $\phi = (1 - \beta)(1 - \alpha)SW_{\downarrow}exp^{-\eta(\max(z-z_s,0))}$ (W m^{-2}) is the net downward solar radiation penetrating to depth z following the Beer-Lambert law, where η is the light extinction coefficient and z_s is the thickness of surface layer.

2.1.2 Experimental designs

The WRF-Lake model encompasses three one-way nested domains with the horizontal resolutions of 50 km, 10 km, and 2 km from Domain 1 to Domain 3 (Fig. 1a). The model domains are centered at (30.7° N, 90.7° E) with 30 sigma levels in the vertical direction and consist of 100×100, 146×146, and 261×246 grid points (number of grids in the west–east direction multiplies that in south-north direction), respectively. The main physical parameterization schemes are listed in Table 1 and the cumulus convection scheme is turned off in Domain 3. The initial and lateral boundary conditions of atmosphere are generated from the 6-h ERA-Interim reanalysis data with a grid spacing of 0.75°×0.75° in longitude/latitude (https://apps.ecmwf.int/datasets/data/interim-full-daily, Simmons et al. 2007). The daily real-time global sea surface temperature dataset with a 0.5°×0.5° resolution (ftp://polar.ncep.noaa.gov/pub/history/sst/rtg_low_res/, Thiebaux et al. 2003) provides the oceanic boundary conditions. The Moderate Resolution Imaging

Table 1 WRF-Lake parameterization schemes

Physics	Scheme
Microphysics	WRF single-moment 6-class (Hong and Lim 2006)
Land surface model	Noah (Mitchell et al. 2005)
Cumulus scheme	Grell–Devenyi ensemble (Grell and Devenyi 2002)
Planetary boundary layer	Yonsei University (Hong et al. 2006)
Shortwave radiation	Dudhia (Dudhia 1989)
Longwave radiation	Rapid radiative transfer model (Mlawer et al. 1997)

Spectroradiometer (MODIS) land-use categories with a resolution of 10 arc seconds (Friedl et al. 2010) provide the land surface types at each model grid. The global lake database version 2 (GLDBv2) including the lake location and depth with the horizontal resolution of 1 km developed by Kourzeneva (2010), Kourzeneva et al. (2012) and Choulga et al. (2014) (available at https://www.flake.igb-berlin.de/ep-data.shtml) gives the ratio of sub-grid lake area to the grid area (lake area/grid area, hereafter represented by lake fraction) and the lake depth at each domain grid (Fig. 1c and d). As the depth of Lake Nam Co is missing in the GLDBv2 dataset, it is updated by the observed bathymetry data (Fig. 1b) provided by Wang et al. (2009).

The air-lake coupled WRF-Lake with the default lake schemes is applied in the outer two domains, and the temperature, humidity and horizontal wind fields above the planetary boundary layer of Domain 1 are nudged to the ERA-Interim reanalysis. The model outputs from an outer domain are employed to generate the initial and boundary conditions for the next-level inner domain. The one-way nesting method inhibits the feedback from Domain 3 to the outer domains. The detailed parameter adjustments are presented in the following Sect. 2.2 and the related configurations of the sensitivity experiments are listed in Table 2. All the experiments run from May 20th to August 31st in 2013. The first 12 days are for spin-up and the results for summer months (June–July–August, JJA) are analyzed.

2.2 Lake scheme modifications

To improve the WRF-Lake model's capability in reproducing the lake thermodynamics and therefore the lake climatic effect over central TP (D03), we evaluated and modified the following lake model parameters based on the different properties between plain fresh lakes and Lake Nam Co. The alpine lakes over central Tibetan share similar characteristics that are different from those of plain freshwater lakes, i.e., the colder and thermally mixed lake temperature in early May, a smaller Tdmax influenced by water salinity and lower surface air pressure, and higher water clarity under the less anthropogenic contaminations. Hence, the

following parameter settings determined by the observed lake properties of Lake Nam Co are transferred to the other lake basins in D03.

2.2.1 Lake temperature profile initialization

In the default lake model, the lake temperature of the top layer is initialized with the input surface skin temperature generated by the avg_tsfc module utility program in WRF (Maussion et al. 2013). The initial lake temperature is assigned with the Tdmax (4 °C) for layers below 50 m, and is calculated according to the surface skin temperature, Tdmax (4 °C) and different layer depth for layers above 50 m. This method is based on the shape of the observed lake temperature profile for Lake Superior in September 1st, 2008 (Gu et al. 2015). Based on the in-situ observation at Lake Nam Co provided by Wang et al. (2019), the entire lake body is well mixed and water temperature from top to bottom exhibits small differences at the start time of the simulations (May 20th, 2013). Hence, for the experiments except the control (CTRL) run, we initialize all vertical layers of Lake Nam Co with the value 2.5 °C, which is calculated by averaging the observed temperatures of different lake layers on May 20th, 2013.

2.2.2 Temperature of maximum water density

The temperature of maximum water density (Tdmax) directly corresponds to the heat capacity of hypolimnion and plays an important role in affecting the development of lake thermal stratification. Tdmax is set to 4 °C for plain freshwater lake. This default value may not be applicable to Lake Nam Co because it is an alpine brackish carbonate lake and Tdmax depends on salinity and atmospheric pressure. According to Wang et al. (2019), Tdmax is close to 3.4 °C as indicated by the observed stable deep-water temperature after the formation of thermal stratification, and is close to 3.6 °C based on the empirical calculation using air pressure of 0.57 bars and salinity of 1.7 g/L (Chen and Millero 1986). In our simulations other than CTRL, we set the Tdmax as 3.5 °C.

Table 2 Configurations of WRF-Lake sensitivity experiments

Experiments	Lake temperature initialization	Tdmax (°C)	Surface roughness lengths (mm)	Light extinction coefficient (m^{-1})	Mixing factor m_d
CTRL	Gu et al. (2015)	4	1	η	100
Sen_LTI	Observation	4	1	η	100
Sen_Tdmax	Observation	3.5	1	η	100
Sen_SRL	Observation	3.5	Subin et al. (2012)	η	100
Sen_LEC	Observation	3.5	Subin et al. (2012)	0.8*η	100
Sen_MF	Observation	3.5	Subin et al. (2012)	0.8*η	150

2.2.3 Lake surface roughness length

The roughness length is a key parameter for calculating the surface turbulent fluxes between the lake and the overlying atmosphere. In the default lake model, the surface roughness lengths for momentum (z_{0m}), sensible heat (z_{0h}) and latent heat (z_{0q}) are set as the same constant value according to different lake states, and for unfrozen lake, $z_{0m} = z_{0h} = z_{0q}$ =0.001 m. The offline WRF-Lake evaluation on Lake Nam Co by Huang et al. (2019) demonstrated that replacing the constant lake surface roughness lengths with the parameterization scheme suggested by Subin et al. (2012) can improve the model performance in reproducing the lake thermodynamics during warm seasons. We test this roughness length parameterization scheme in the sensitivity simulations, represented as

$$z_{0m} = \max\left(\frac{0.1\upsilon}{u_*}, C\frac{u_*^2}{g}\right) \geq 10^{-5} \text{ m}, \tag{3}$$

$$z_{0h} = z_{0m}\exp\left\{-\frac{\kappa}{P_r}\left(4\sqrt{R_0} - 3.2\right)\right\} \geq 10^{-5} \text{ m}, \tag{4}$$

$$z_{0q} = z_{0m}\exp\left\{-\frac{\kappa}{S_c}\left(4\sqrt{R_0} - 4.2\right)\right\} \geq 10^{-5} \text{ m}, \tag{5}$$

where υ is the kinematic viscosity of air (m^2 s^{-1}), u_* is the surface friction velocity (m s^{-1}), C is the effective Charnock coefficient, g=9.80616 m s^{-2} is the gravitational acceleration, $R_0 = \max\left(\frac{z_{0m}u_*}{\upsilon}, 0.1\right)$ is the near-surface atmospheric roughness Reynolds number, P_r=0.71 is the molecular Prandt number for air, S_c=0.66 is the molecular Schmidt number for water in air. More details can be found in Subin et al. (2012).

2.2.4 Light extinction coefficient

The distribution of net downward solar radiation at different lake depth depends on the light extinction coefficient, which is related to the degree of lake clarity. In the default lake model, $\eta = 1.1925d^{-0.424}$ is expressed as an empirical function of lake depth (d) according to the data from 88 Swedish lakes (Hakanson 1995), implying that the light extinction coefficient experiences horizontal variability with the varying lake depth across the model grids. As the TP lakes are less contaminated by human activities and contain smaller amount of aquatic plants compared with plain lakes, we consider TP lakes more limpid and scale down the default η by a factor of 0.8 to allow more solar radiation to penetrate into the deep lake layers. In this case, η at the observation site

over Lake Nam Co is decreased from 0.175 to 0.14 m^{-1}, which is closer to the mean estimated value 0.12 m^{-1} in Wang et al. (2009) and has also been used in Lazhu et al. (2016).

2.2.5 Thermal diffusivity

For mitigating the WRF-Lake's underestimation of deep-lake vertical mixing strength and therefore improving the LST simulations over Lake Superior, Gu et al. (2015) increased the wind-driven eddy diffusivity k_e by a factor of 10^2–10^5 based on the different lake depth and surface temperature within the default lake model. For example, k_e is multiplied by m_d = 100 when lake depth exceeds 15 m and T_s is greater than 4 °C. In our simulations, we enlarge k_e using m_d = 150.

2.3 Evaluation data and methodology

The model performances in lake thermal structure are evaluated with the daily lake temperature profile in 2013 measured at a station located at the southeastern part of Lake Nam Co (30°45.74′ N, 90°46.83′ E, denoted by a solid aster symbol in Fig. 1b). The water temperature were measured at depths of 3, 6, 16, 21, 26, 31, 36, 56, 66 and 83 m, with details documented by Lazhu et al. (2016). The simulated wind speed, downward shortwave and longwave radiation over the Lake Nam Co are compared with an hourly forcing data for offline lake modelling (Huang et al. 2019). This dataset was generated by Lazhu et al. (2016) based on the 3-hourly, 0.1°×0.1° dataset from the Institute of Tibetan Plateau Research, Chinese Academy of Sciences (ITPCAS, available at https://en.tpedatabase.cn/portal/; Chen et al. 2011; He et al. 2020) and the observation data collected at the meteorological station on the northeastern shore of Lake Nam Co (Fig. 1b). The modelled LST is assessed against the MODIS product (MOD11A1) with a spatial resolution of 1 km (available at https://modis.gsfc.nasa.gov/data/dataprod/mod11.php, Wan et al. 2004), which provides the LST over Lake Nam Co at approximately 11:00 and 21:00 local time. Following Dai et al. (2018a), we only employ the nighttime data for LST evaluation because the nighttime retrieval from satellite remote sensing is more accurate due to the absence of strong solar heating bias (Hook et al. 2003). The model simulated 2-m air temperature (hereafter denoted as T_{2m}) is compared against the ITPCAS data, and the precipitation is verified by both the ITPCAS and the Tropical Rainfall Measuring Mission 3B42 datasets (hereafter abbreviated as TRMM3B42, available at ftp://disc2.nascom.nasa.gov/data/ TRMM/Gridded, Huffman et al. 2007). In addition, the hourly, 0.25°×0.25° ERA5 reanalysis data (available at https://cds.climate.copernicus.eu) is utilized to provide the summer atmospheric circulation information over TP.

Specifically, the model simulated LST and water temperature profile for evaluation are taken at the grid point nearest to the Nam Co Station, with the lake depth to be 91.3 m according to the model grid and to be 93 m at the station (Wang et al. 2019). The simulated 25-layer water temperature is linearly interpolated onto the depths of the observational data. Four statistics including the mean bias (BIAS), the root-mean-square error (RMSE), the Pearson temporal/pattern correlation (TC/PC), and the Taylor score (TS) are utilized for the model assessment. The above verification statistics are estimated according to

$$\text{BIAS} = \frac{1}{N} \sum_{i=1}^{N} (S_i - O_i), \tag{6}$$

$$\text{RMSE} = \sqrt{\frac{1}{N} \sum_{i=1}^{N} (S_i - O_i)^2}, \tag{7}$$

$$\text{TC/PC} = \frac{\sum_{i=1}^{N} (S_i - \overline{S})(O_i - \overline{O})}{\sqrt{\sum_{i=1}^{N} (S_i - \overline{S})^2} \sqrt{\sum_{i=1}^{N} (O_i - \overline{O})^2}}, \tag{8}$$

$$\text{TS} = \frac{4(1 + TC)}{(\sigma + 1/\sigma)^2 (1 + TC_0)}, \tag{9}$$

$$\sigma = \sqrt{\frac{1}{N} \sum_{i=1}^{N} (S_i - \overline{S})^2} \Big/ \sqrt{\frac{1}{N} \sum_{i=1}^{N} (O_i - \overline{O})^2}, \tag{10}$$

where $S_i(O_i)$ denotes the simulated (observed) values with a total of N samples in time or in space; $\overline{S}$ ($\overline{O}$) represents the average of $S_i(O_i)$ over N points; σ is the temporal/spatial standard deviation of the simulated values normalized by that of the observed values; and $TC_0 = 1$ is the achievable maximum temporal/spatial correlation. Higher TC indicates greater similarity in temporal/spatial variation between the simulated and observed values, while lower RMSE indicates that the simulated values are more consistent with the observed values in quantity. As documented in Taylor (2001), TS can quantify how the simulated values match the observed values in terms of both the temporal/spatial pattern and amplitude, and better model performance can be indicated by a large TS closer to the achievable maximum value 1.

Additionally, we utilize the equivalent potential temperature θ_e to describe the atmospheric stability:

$$\theta_e = \left(T + \frac{L_v q_v}{C_p} \right) \left(\frac{P_{ref}}{P} \right)^{\frac{R}{C_p}}, \tag{11}$$

where T is the air temperature, L_v is the latent heat of evaporation (2.5×10^6 Jkg^{-1}), q_v is the specific humidity, C_p is the specific heat capacity of air at constant pressure (1005 Jkg^{-1} K^{-1}), P_{ref} is the standard atmospheric pressure (1×10^5 Pa), and P is the air pressure.

3 Results

## 3.1 Control simulation with the default lake scheme

During the simulation period (May 20th to August 31st, 2013), the observed epilimnion temperature almost exhibits an identical value from the lake surface to 6 m depth (Wang et al. 2019). Thus, we employ both the LST and the lake temperature at 3 m depth (hereafter denoted as TLake$_{3m}$) to evaluate WRF-Lake's performance in simulating the lake surface layer temperature. Figure 2a and b compares the CTRL simulated nighttime LST (daily TLake$_{3m}$) versus that in MODIS data (in-situ observations). According to observations, the lake surface layer temperature of Lake Nam Co ranges from 3° to 12 °C and exhibits a continuous warming trend during summer. The WRF-Lake with default lake schemes reasonably reproduces the temporal evolution of near-surface lake temperature with a TC of 0.84 (0.96) in comparison with the MODIS (in-situ) data. However, CTRL overestimates the LST by a maximal BIAS of 6.07 °C (3.27 °C) relative to the MODIS (in-situ) data before mid-July, and underestimates the LST from then on. The RMSE against the MODIS (in-situ) data is 2.15 °C (1.13 °C).

The radiative forcing is the primary input energy for the entire lake system and plays an important role in determining the equilibrium temperature at the lake–atmosphere boundary (Jimenez et al. 2014). From Fig. 2c and d, the biases between the modeled and observed downward shortwave radiation (longwave radiation) are 39.3 W m^{-2} (-4.4 W m^{-2}), suggesting that the atmospheric fluxes generated by WRF are within a plausible range (Xu et al. 2016) and the errors of the simulated LST are mainly resulted from the inaccurate lake physical processes depicted by the default lake scheme in the WRF-Lake model.

3.2 Lake surface temperature from simulations with improved lake scheme

To reveal the influences of the calibrated lake model parameters on LST simulations, the summer daily time series of TLake$_{3m}$ from the in-situ observations and each model simulation are shown in Fig. 3, and the quantitative performances
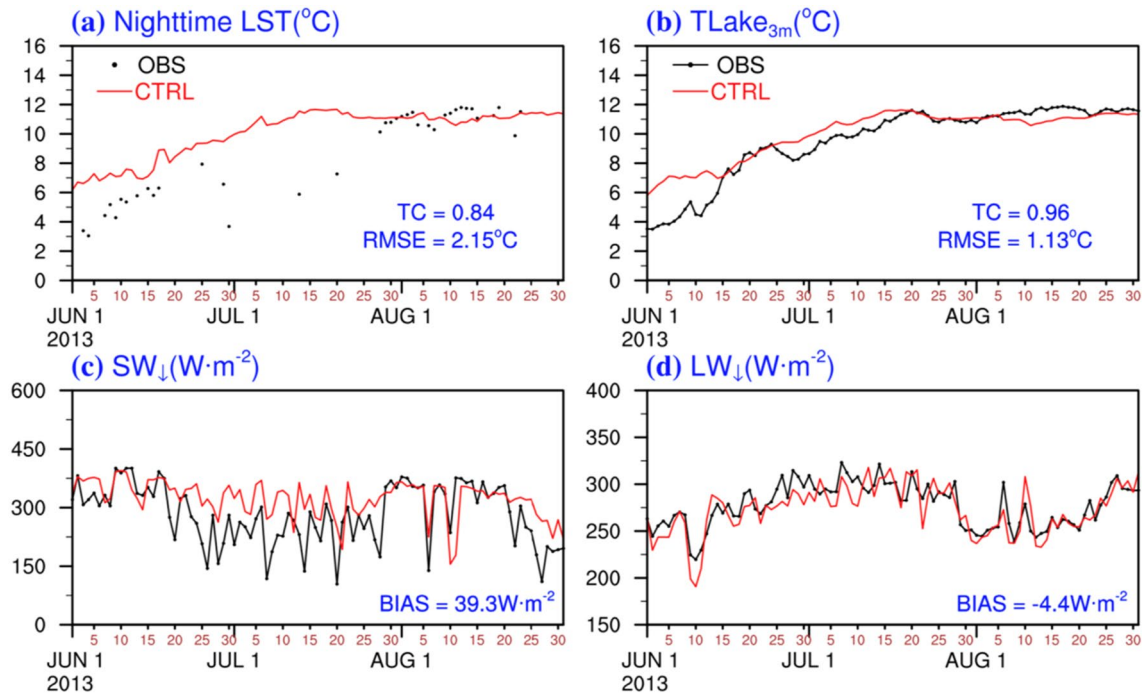
Fig. 2 The daily observed (black dots or lines) and CTRL simulated (red lines) **a** nighttime LST (unit: °C), **b** TLake$_{3m}$ (water temperature at 3 m depth) (unit: °C), **c** downward shortwave radiation (SW$_\downarrow$, unit: W m^{-2}), and **d** downward longwave radiation (LW$_\downarrow$, unit: W m^{-2}) during June 1st to August 31st 2013. The temporal correlation (TC) and root-mean-square-error (RMSE) between the simulations and observations for LST and TLake$_{3m}$ are presented in **a** and **b**, and the BIAS between modeled and observed SW$_\downarrow$ and LW$_\downarrow$ are presented in **c** and **d**
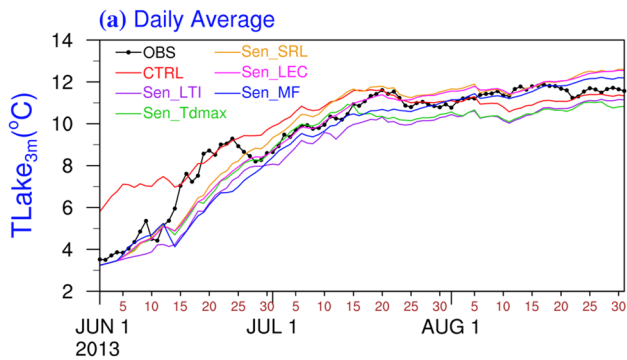
Fig. 3 The daily TLake$_{3m}$ (unit: °C) from the station measurements and the simulations at the observation site during June 1st to August 31st 2013

of the simulations are illustrated in Fig. 4. Obviously, the simulated TLake$_{3m}$ is sensitive to changes in lake model parameters.

From Fig. 3, it is obvious that the overestimated TLake$_{3m}$ in CTRL during June to mid-July is related to the unrealistically higher initial water temperature profile, which also results in the incorrectly earlier onset of the lake thermal stratification (Fig. 5). By initializing the water column temperature with the observed water temperature (2.5 °C) averaged over different lake water layers, the Sen_LTI experiment with less initial thermal storage obtains TLake$_{3m}$ in better agreement with observations, as indicated by the slight increase in TC and the significant increase in TS by 0.19 (Fig. 4). Sen_LTI underestimates the summer TLake$_{3m}$ with a BIAS (RMSE) of − 0.98 °C (1.13 °C).

The intensified solar heating in May–June leads to the springtime warming from the original thermally mixed state in Lake Nam Co. Before the LST reaching Tdmax, the eddy diffusivity is enlarged by 10^4 times (Gu et al. 2015), and thus a large portion of the incoming radiative heat flux is transferred into the deeper lake layers, causing the water column temperature increasing with a rather uniform rate until the hypolimnetic temperature reaches Tdmax. Thus, a decreased Tdmax can reduce the hypolimnetic thermal storage and also fasten LST's ascending speed in response to the radiative forcing at the beginning of springtime warming. From Fig. 3, by adjusting the Tdmax from 4 °C for the freshwater lake to the observed 3.5 °C in Lake Nam Co, the Sen_Tdmax experiment effectively increases the warming amplitude of TLake$_{3m}$ from early June to mid-July. Compared with Sen_LTI, the Sen_Tdmax experiment obtains summer TLake$_{3m}$ that agrees better with observations, with RMSE (BIAS) of 0.93 °C (− 0.68 °C), while 1.13 °C (− 0.98 °C) for Sen_LTI.
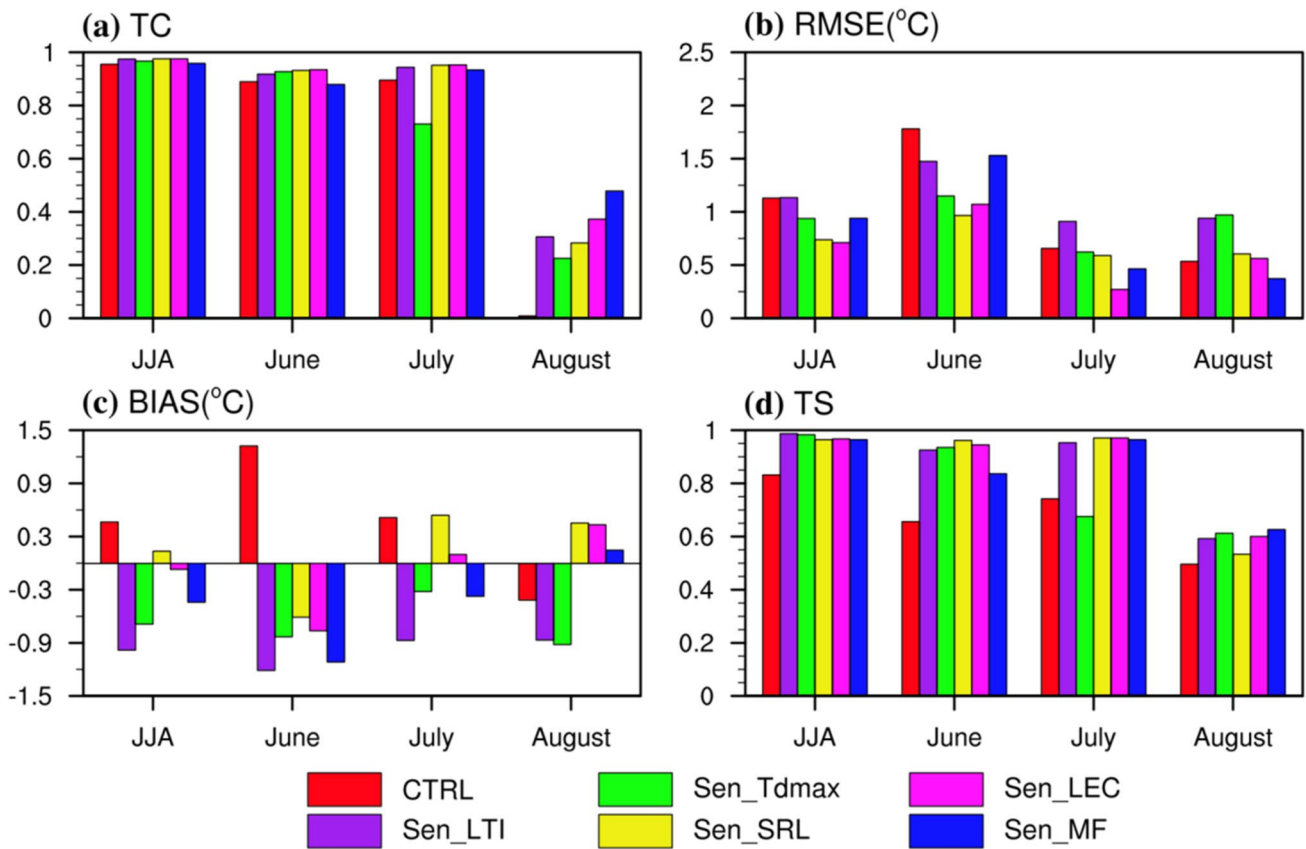
Fig. 4 **a** TC, **b** RMSE (unit: °C), **c** BIAS (unit: °C), and **d** TS between the simulated and the observed daily $TLake_{3m}$ during June–July–August (JJA, summer) and the individual month of summer in 2013

As discussed in many previous studies (Dai et al. 2018c; Xu et al. 2016; Wang et al. 2018), the default surface roughness length for unfrozen lake is often too large, thus inducing unrealistically strong wind-driven mixing right below the lake–atmosphere interface, excessive loss of latent heat flux and the underestimation of LST. In the Sen_SRL experiment, the parameterized roughness length with a dynamical range of 0.1–0.5 mm is used to better represent the lake–air interactions. Compared with Sen_Tdmax, the Sen_SRL experiment obtains a significantly increased $TLake_{3m}$ (Fig. 3), which is largely due to the decreased latent and sensible heat fluxes. The RMSE (BIAS) of summer $TLake_{3m}$ in Sen_SRL experiment is 0.74 °C (0.14 °C), reduced from 0.93 °C (− 0.68 °C) in Sen_Tdmax run (Fig. 4). Sen_SRL overcorrects $TLake_{3m}$, with a mean positive BIAS of 0.49 °C during July and August.

The light extinction coefficient and eddy diffusivity are two key parameters determining the distribution and transmission of the sub-surface heat fluxes, and therefore the vertical distribution of lake temperature. In general, more solar radiation penetrates into and heats the deep-water layers with the decreasing η, resulting in lower LST, a warmer mixolimnion, and a deepened thermocline. With a decreased η in the

Sen_LEC experiment, the BIAS of $TLake_{3m}$ in July significantly decreases to 0.09 °C, from 0.54 °C in the Sen_SRL experiment (Figs. 3 and 4). The RMSE (BIAS) of summer $TLake_{3m}$ in Sen_LEC is 0.71 °C (− 0.07 °C), reduced from 0.74 °C (0.14 °C) in Sen_SRL. For depicting the strong turbulent water mixing in deep lakes, k_e was significantly enlarged by a mixing factor (m_d) in previous studies (Martynov et al. 2012; Subin et al. 2012; Xiao et al. 2016), and larger m_d values lead to more heat transfer from the near-surface water to the deep lake body. By enhancing the eddy diffusivity with $m_d = 150$ in the Sen_MF run, the RMSE (BIAS) of summer $TLake_{3m}$ is 0.94 °C (− 0.44 °C), larger than 0.71 °C (− 0.07 °C) in the Sen_LEC experiment using $m_d = 100$. This indicates that $m_d = 100$ better represents the vertical mixing strength at the deep layers of Lake Nam Co.

### 3.3 Vertical temperature profile simulations with improved lake scheme

To reveal the impacts of the tuned model parameters on simulating the onset of thermal stratification and the vertical distribution of water temperature, Fig. 5 shows the time-depth distributions of the daily observed and the

Fig. 5 Time-depth distributions of the daily mean water temperature (unit: °C) from **a** the station measurements and **b**–**g** the simulations at the observation site during June 1st to August 31st 2013. The black dashed lines indicate the onset of lake thermal stratification
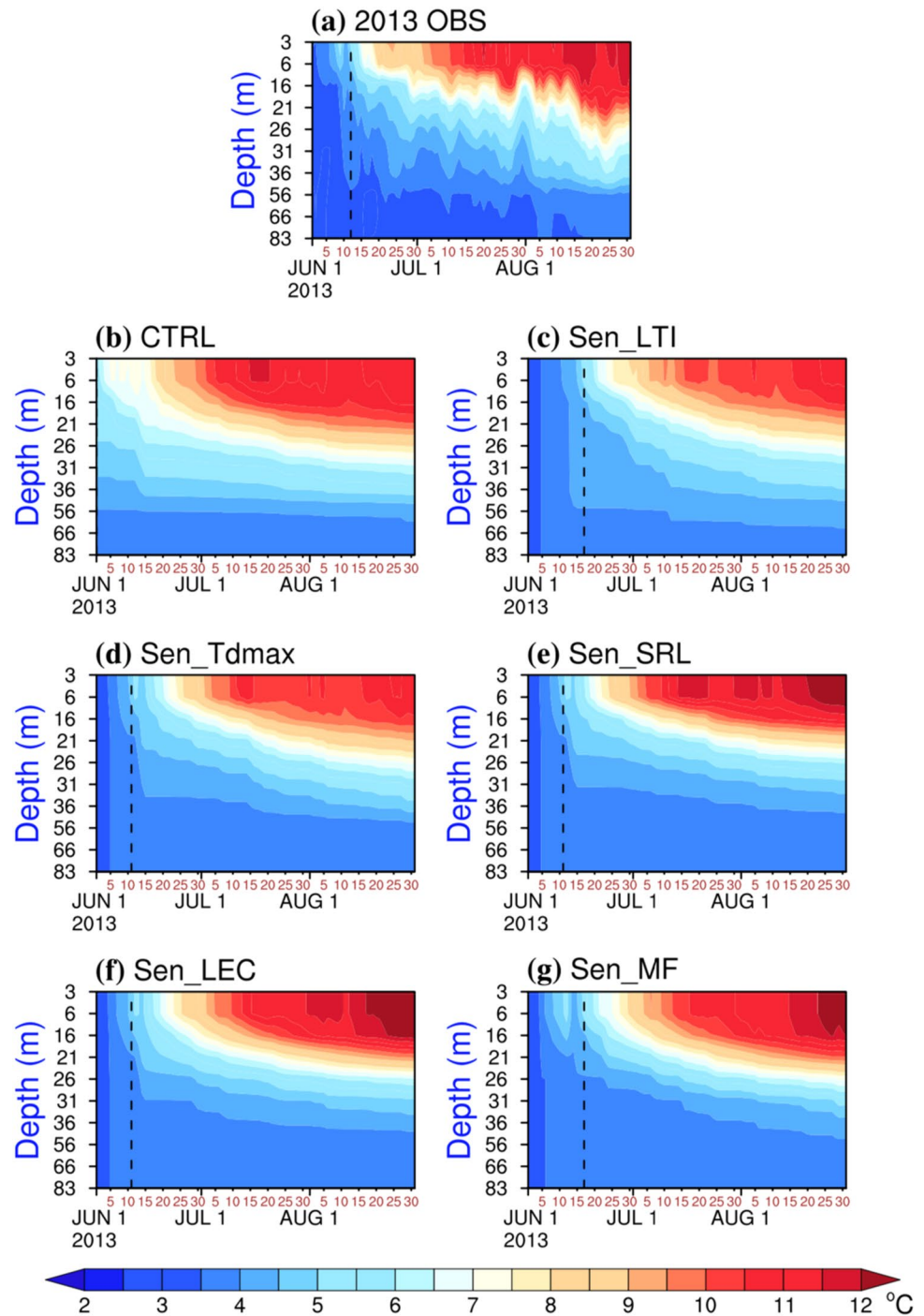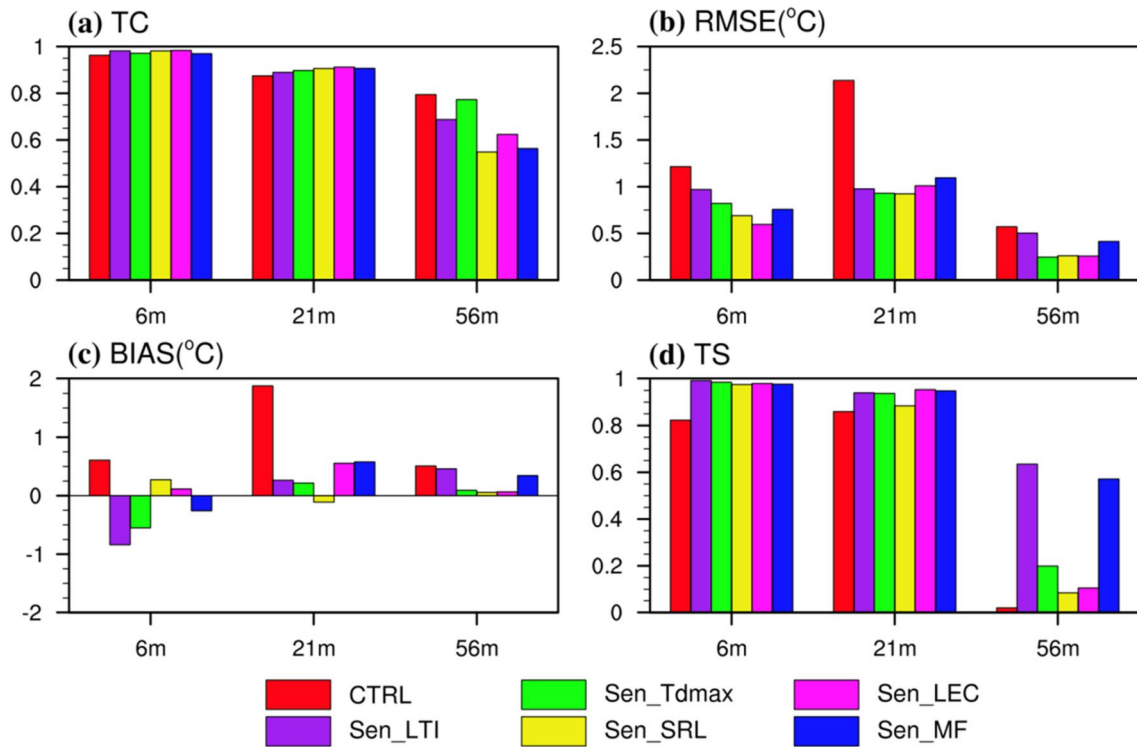

modelled water temperature during summer in 2013. Figures 6 and 7 exhibit model's quantitative performance in simulating the water temperature variations at mixolimnion, metalimnion, and hypolimnion at 3 representative lake depths (6 m, 21 m, and 56 m). The onset of lake thermal stratification is defined as the first date from which the temperature differences between 6 and 56 m depths are greater than 1 °C in the subsequent 4 days without exception (Wang et al. 2019).

According to observations (Fig. 5a), the lake water temperature slightly decreases from the lake surface to deep layers until the establishment of the lake thermal stratification on June 12th. As a result of the enhanced solar heating from then on, the upper mixed layer gradually warmed and deepened to ~26 m along with the development of thermocline. In general, the evolution features of the vertical temperature profile are reasonably reproduced by all the experiments except for the CTRL run (Fig. 5), which
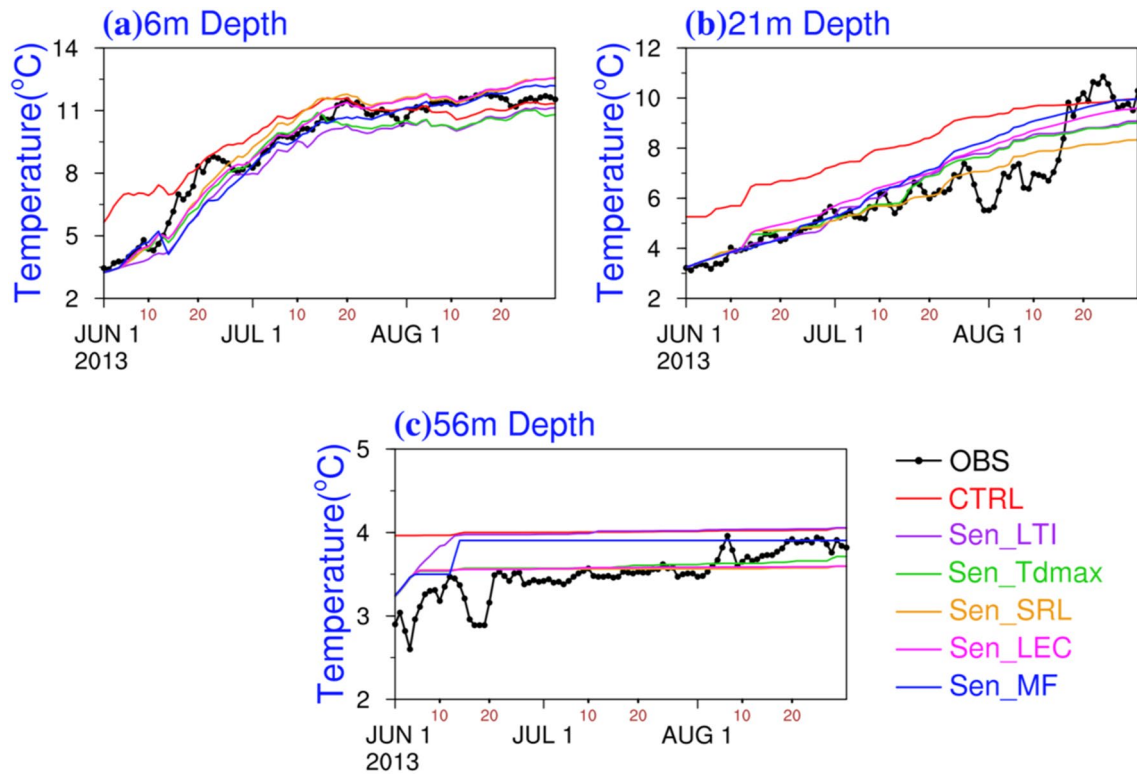
Fig. 6 The daily evolution of the observed and modeled water temperature (unit: °C) at **a** 6 m, **b** 21 m, and **c** 56 m lake depth in the observation site during June 1st to August 31st 2013

Fig. 7 a TC, **b** RMSE (unit: °C), **c** BIAS (unit: °C), and **d** TS between the simulated and the observed water temperature at depths of 6 m, 21 m, and 56 m during summer in 2013

largely overestimates the whole lake body temperature and obtains an incorrectly earlier thermal stratification development due to the higher initial water column temperature. Compared to CTRL, the Sen_LTI experiment with a realistic initial water temperature (2.5 °C) postpones the onset of thermal stratification on June 17th (Fig. 5b and c). Comparison between Sen_LTI and Sen_Tdmax demonstrates that the tuned Tdmax, which made the model more realistic in depicting the stability threshold for lakes to adjust their subsurface thermal structure, results in a more accurate onset of summer thermal stratification on June 11th (Fig. 5c and d). Further model modifications lead to little improvement on the simulated onset of thermal stratification, but influence the water temperature simulations at different lake depth during the stable stratified period.

From Figs. 6 and 7, the lake model's accuracy in reproducing the amplitude and pattern of water temperature variability decreases with the increasing lake depth. At 6 m depth, all experiments perform well in the temporal evolution of water temperature and the pattern and amplitude of the temperature variability with the TC/TS values greater than 0.8, while their capability in quantitatively reproducing the lake temperature varies greatly. By adjusting the initial water column temperature, Tdmax, surface roughness length, and light extinction coefficient one by one from Sen_LTI to Sen_LEC, the WRF-Lake model's ability in simulating the epilimnetic temperature is significantly improved with the RMSE (BIAS) value reduced from 0.97 °C (− 0.84 °C) to 0.59 °C (0.11 °C). From Fig. 6b and c, the observed lake temperature evolutions at 21 m and 56 m depths show a fluctuant ascending trend, which is due to the simultaneous influences of the enhanced convective mixing and the active internal wave motions across the thermocline. However, due to the missing representations of the complex lake interior hydrodynamic processes in the 1-D WRF-Lake, all the simulations fail to depict the variations of metalimnion and hypolimnion temperature indicated by the lower TS values. In terms of the verification statistics including RMSE and BIAS, the Sen_SRL experiment shows relatively better performances in simulating the temperature at 21 m and 56 m depths.

### 3.4 Impacts of the improved lake scheme on atmospheric component

The above evaluation results reveal the improvements in simulating the lake thermodynamics, especially the near-surface water temperature, through using the calibrated lake scheme in the coupled WRF-Lake model. This may lead to improvement in the simulated water and heat exchanges between the lake surface and the overlying atmosphere. In this section, the T_{2m} and precipitation simulated by the CTRL and Sen_LEC runs are compared for demonstrating

the effects of the improved LST on regional climate modelling. A sub-region bounded by 30° N–31.5° N and 90° E–91.5° E (i.e. the red rectangle in Fig. 8a) is selected for focusing on the comparisons surrounding Lake Nam Co.

From Fig. 8a–c, both the CTRL and Sen_LEC experiments can reasonably capture the general spatial patterns of the summer mean T_{2m} over central TP, except for some cold (warm) biases in the southern mountainous areas (northern lower lands). As the CTRL run predicts an unrealistically higher near-surface water temperature, the related upward water and heat fluxes are overestimated, leading to positive T_{2m} simulation biases over the lake and surrounding regions (Fig. 8b and d). With the improvement in the modelled LST, the summer mean over-lake T_{2m} in Sen_LEC is overestimated by 1.4 °C, reduced from 1.71 °C in the CTRL run (Fig. 8d–f). The T_{2m} simulation over the sub-region is also improved in terms of PC, TS, and RMSE (Table 3).

During the boreal summer, the dominant southwesterly monsoon circulation plays an important role in modulating the TP climate and contributes to the southeast-northwest precipitation gradient over the TP (Fig. 9a) (Maussion et al. 2013). From Fig. 9b and c, both the CTRL and Sen_LEC experiments can generally reproduce the 500 hPa wind fileds over Domain 3, and predict the summer mean precipitation with the TS values of 0.79 and 0.80, respectively. From Fig. 9d and e, both experiments overestimate (underestimate) the rainfall surrounding (over) the Lake Nam Co. The overestimated rainfall around the Nyainqentanglha Mountain and the regions downwind the lake (marked by the blue rectangle in Figs. 9f and 10f) is reduced from CTRL to Sen_LEC, which is attributed to the disparate lake-effect strength. Previous studies have demonstrated that due to the large water vapor supply, the warm surface lake water and the small water surface roughness length in summer, the prevailing southwest wind passing the Lake Nam Co can be accelerated, moistened, and warmed by the underlying water surface (Dai et al. 2018a; Wu et al. 2019). Additionally, under the superimposed impact of mountain-valley wind induced by the sharp orographic contrast, the warm and moist wind would be further amplified and then converge and ascend over the lake and downwind regions, promoting more convective developments therein. By mitigating the LST overestimation in the CTRL run, the Sen_LEC experiment predicts reduced upward moisture and heat fluxes that support the convective stimulation, and thus the decreased lake-effect precipitation strength. The 500 hPa wind filed differences between Sen_LEC and CTRL experiments show divergent flow patterns over the regions downwind the lake, and a reduced positive rainfall bias in the Sen_LEC run (Fig. 8f). Further comparisons between the simulated results and the ITPCAS rainfall dataset also demonstrate that the Sen_LEC experiment can effectively weaken the lake's excessive warming and moistening impacts modeled by CTRL run,
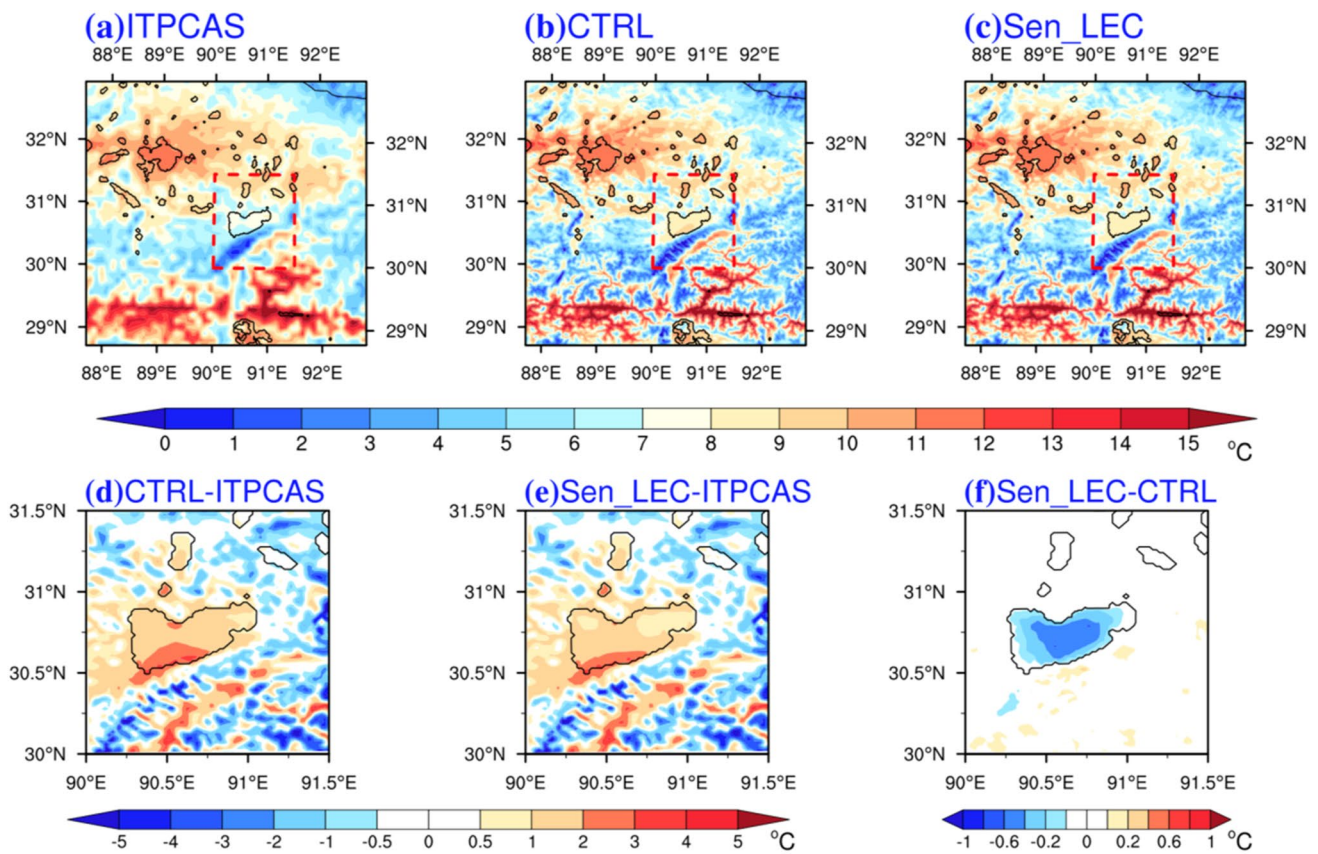
Fig. 8 The summer mean **a** ITPCAS observed, **b** CTRL, and **c** Sen_LEC simulated T_{2m} (unit: °C) over the Domain 3 during 2013. Bottom panel contains the corresponding T_{2m} differences of **d** CTRL-ITPCAS, **e** Sen_LEC-ITPCAS, and **d** Sen_LEC-CTRL over the sub-region (30° N–31.5° N, 90° E–91.5° E) indicated by the red rectangle in (**a**–**c**). The black curves in (**a**–**f**) outline the locations and ranges of TP lakes

Table 3 The pattern correlation (PC), Taylor score (TS), and root-mean-square-error (RMSE) between the simulations and observations for the T_{2m} and precipitation over the sub-region (30° N–31.5° N, 90° E–91.5° E)

Variables	Experiments	Statistics		
		PC	TS	RMSE
T_{2m}	CTRL	0.82	0.86	1.53 °C
	Sen_LRC	0.83	0.87	1.50 °C
Precipitation	CTRL	0.68	0.67	1.13 mmd^{-1}
	Sen_LRC	0.70	0.70	1.00 mmd^{-1}

and thus mitigate the rainfall overestimation around the Nyainqentanglha Mountain and the regions downwind the lake (Fig. 10). Overall, the Sen_LEC experiment improves the simulation of the summer mean rainfall over the sub-region in terms of PC, TS, and RMSE (Table 3).

As the precipitation over the regions downwind the lake (30.7–31.2° N, 90.81–91.33° E) is significantly influenced by the lake-induced downwind enhancement impacts (Dai et al. 2018a, b; Wu et al. 2019), we select this area to explore the influences of the improved lake–air interactions on modeling the rainfall diurnal variations. The intercomparisons between the diurnal cycles of the regional averaged rainfall from TRMM, ITPCAS, CTRL and Sen_LEC during summer of 2013 are presented in Fig. 11. From the 3-hourly TRMM and ITPCAS data, the rainfall diurnal variation downwind the Lake Nam Co is characterized by a pronounced late-afternoon peak (18 local solar hour, hereafter denoted as LSH) and the relatively larger values from night to early morning. Both the CTRL and Sen_LEC experiments predict a delayed dominant late-afternoon rainfall peak (19 LSH) and overestimate the rainfall during daytime and nighttime. Compared with the CTRL results, Sen_LEC tends to mitigate the general rainfall overestimation and better predict the nighttime rainfall (19–23 LSH) due to the more realistic representations of LST and turbulent water/heat exchanges. However, the WRF-Lake with a calibrated lake scheme still exhibits evident positive biases in modeling the daytime rainfall. Given that the rainfall diurnal variation is a synthesized climatic phenomenon modulated by
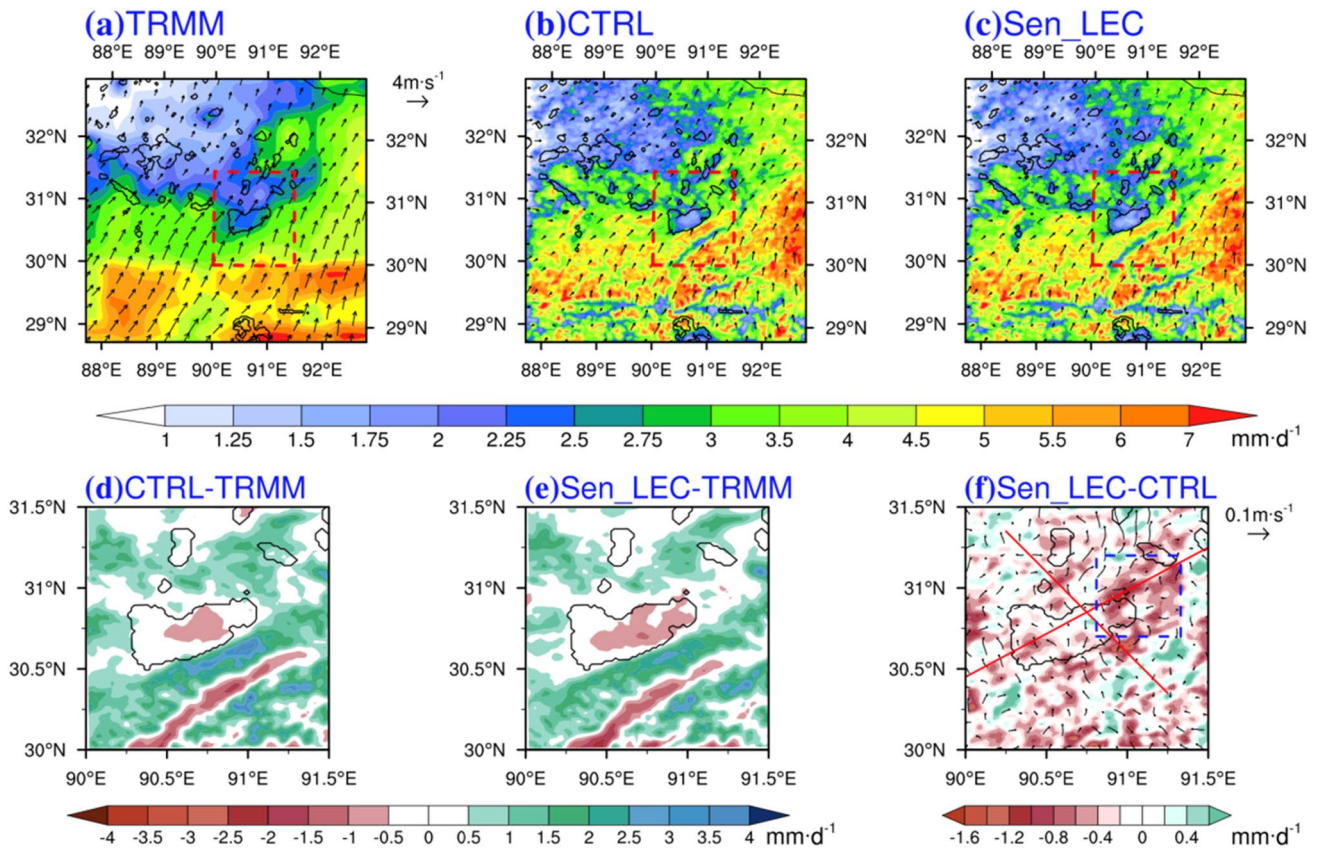
Fig. 9 The mean **a** TRMM observed, **b** CTRL, and **c** Sen_LEC simulated precipitation (unit: mm day⁻¹) over the Domain 3 during summer in 2013. Bottom panel contains the corresponding precipitation differences of **d** CTRL-TRMM, **e** Sen_LEC-TRMM, and **d** Sen_LEC-CTRL over the sub-region indicated by the red rectangle in **a**–**c**. The vectors are the summer mean wind fields at 500 hPa (unit: m s⁻¹) from **a** ERA5 reanalysis, **b** CTRL simulations, **c** Sen_LEC simula-tions, and **f** Sen_LEC-CTRL differences, respectively. The black curves in (**a**–**f**) outline the locations and ranges of TP lakes. In (**f**), the blue dashed rectangular denotes the regions downwind the lake (30.7–31.2° N, 90.81–91.33° E), and the red lines represent the transections used for lake–downwind and lake–mountain vertical cross sections in Fig. 12

the diurnal evolution of boundary layer properties and large-scale atmospheric forcing (Dai and Trenberth 2004; Yang et al. 2017), the current daytime rainfall overestimation may be attributed to the uncertainties from the other physical processes in the coupled WRF-Lake. This points out that more assessments on WRF-Lake's physical processes are needed for expanding the model's applicability on TP climatic simulations.

To further understand the underlying mechanisms of the improved T_{2m} and precipitation simulations, we investigate the disparate atmospheric responses to different LST patterns modeled by the CTRL and Sen_LEC experiments along two vertical transections (Fig. 12), which are indicated by the red lines in Fig. 9f. The southwest-northeast transection crossing the Lake Nam Co and the downwind regions is denoted as Lake–Downwind, and the northwest–southeast transection crossing the Lake Nam Co and the Nyainqentanglha Mountain is denoted as Lake–Mountain. Compared with CTRL, the Sen_LEC

experiment mitigates the LST overestimation, weakens the upward water and heat fluxes, and obtains a older and drier overlying atmosphere around Lake Nam Co (Fig. 12a–d). The lake-induced anomalous cooling and desiccating effects can reinforce each other in generating the stable boundary layer up to ~ 5.8 km and inhibit the convective developments around the Lake Nam Co (Fig. 12e and f). At the diurnal timescale, as the over-lake colder and drier air in Sen_LEC could be advected by the lake breeze and valley wind during daytime, the atmosphere column over the surrounding land and mountainous regions is featured by a stable boundary layer and anomalous katabatic motions. This explains the mitigated rainfall overestimation over these regions in the Sen_LEC run. During nighttime, the colder LST simulated by Sen_LEC weakens the lake–land thermal contrast and the over-lake ascending motions, resulting in less rainfall in the central lake regions (Fig. 9d–f).
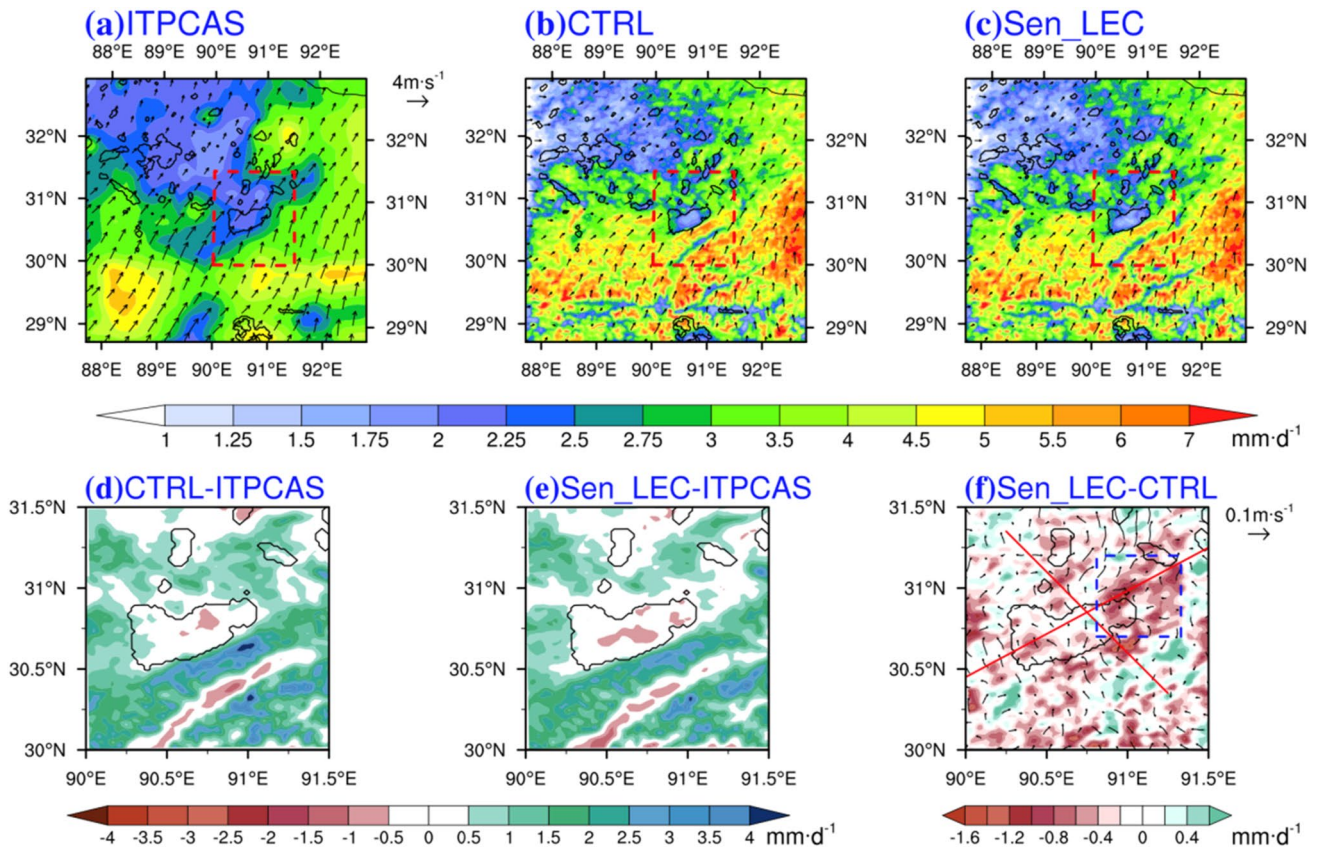
Fig. 10 Same as Fig. 9, but for the comparisons of summer mean rainfall spatial distributions from ITPCAS datasets, CTRL, and Sen_LEC experiments
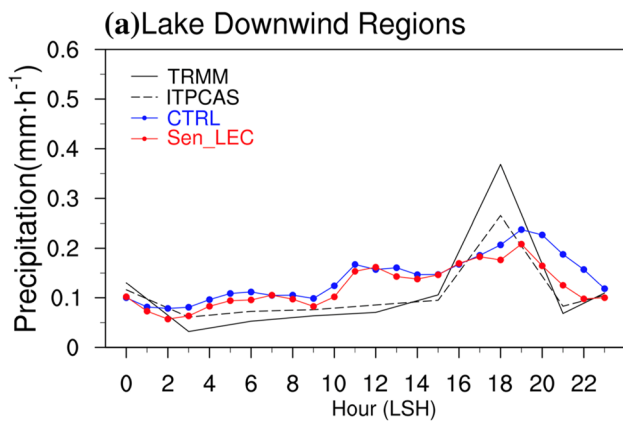
Fig. 11 The diurnal cycles of rainfall averaged over the lake downwind regions from TRMM, ITPCAS, CTRL, and Sen_LEC during summer in 2013. The X axis is local solar hour (LSH)

4 Summary and discussion

Based on the in-situ observation data at Lake Nam Co, we evaluate and calibrate the coupled WRF-Lake from the perspective of model's performance in simulating the LST and the evolutions of vertical temperature profiles during summer. The effects of the improved LST and lake–air interactions on regional climate modelling are also discussed. Main findings are summarized as follows:

During summer, the upper-most water temperature (i.e., the lake temperature at 3 m and 6 m) gradually increases from 3.5° to 12 °C. The whole water column warms slowly and depicts a weak temperature gradient before the onset of stable lake thermal stratification (June 12th). In response to the enhanced solar heating from then on, the epilimnetic temperature rises rapidly with the mixed layer deepening to ~ 26 m, and the simultaneous metalimnion and hypolimnion temperature exhibit fluctuant rising features. However, the coupled WRF-Lake model with default lake scheme parameters predicts excessively warmer LST, earlier establishment of lake thermal stratification and a colder epilimnion during the late summer. By adjusting the initial lake temperature profile, Tdmax, surface roughness length and light extinction coefficient one by one from Sen_LTI to Sen_LEC experiments, WRF-Lake model's capability in reproducing the evolutions of LST and vertical temperature profiles in Lake Nam Co is improved. The RMSE (BIAS)

Fig. 12 The height-latitude lake–downwind (left) and lake–mountain (right) cross sections of the simulated summer mean differences (Sen_LEC-CTRL) in the air temperature (top), specific humidity (middle), and equivalent potential temperature (shaded) with the longitudinal circulation (vectors, units: m s^{-1}) (bottom) during 2013. The vertical velocity was enlarged by 70 times. The gray shaded areas in (**a**–**f**) denote the absolute terrain height above sea level. The sunken areas marked by the blue dashed lines and stars in (**a**–**f**) roughly represent the locations of Lake Nam Co
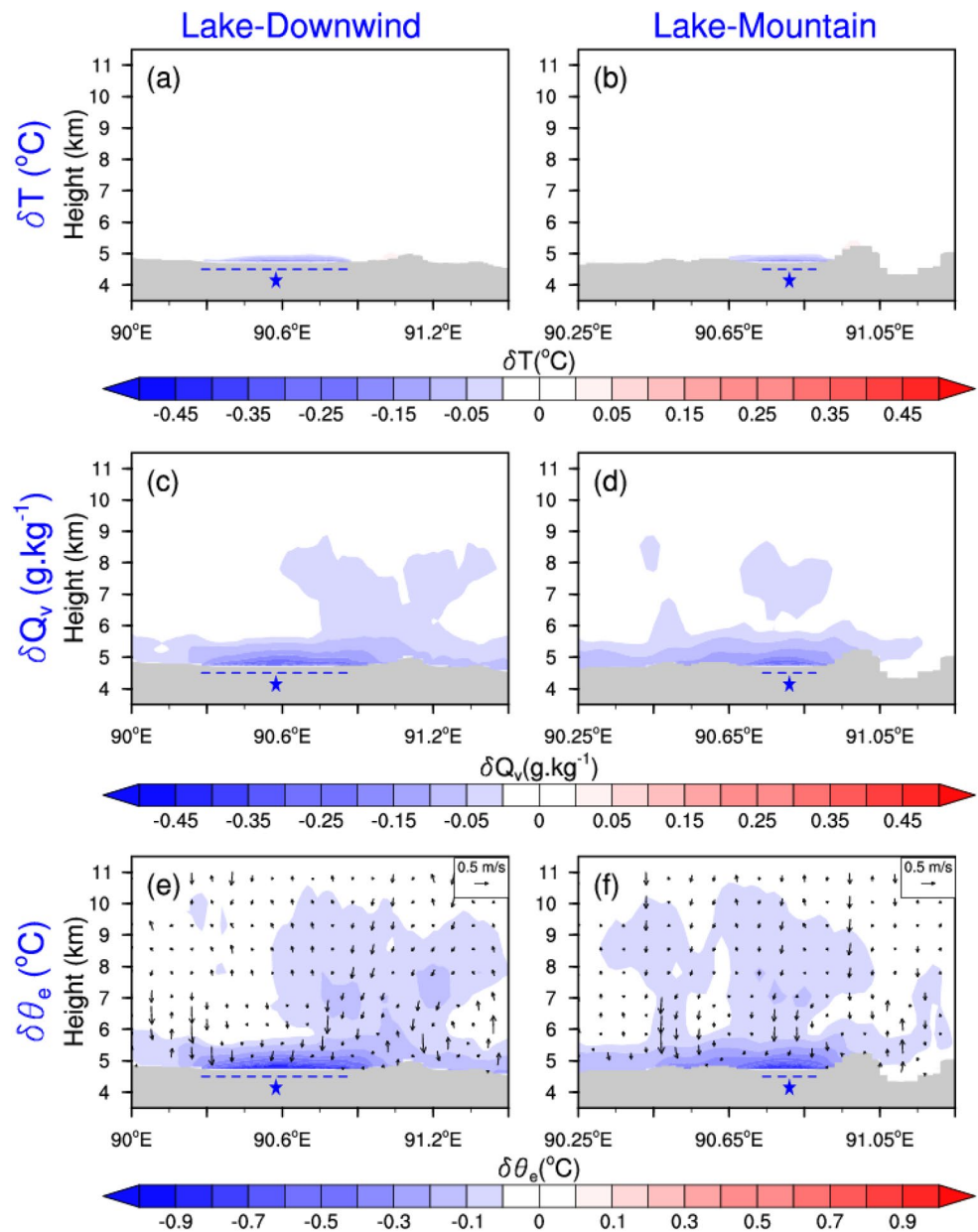
of summer TLake$_{3m}$ in Sen_LEC experiment is 0.71 °C (− 0.07 °C), reduced from 1.13 °C (0.47 °C) in CTRL run. The onset of lake thermal stratification predicted by Sen_LEC (June 11th) is also in better agreement with observations (June 12th). Benefited from the more realistic simulations in the near-surface water temperature and lake–air interactions, the calibrated WRF-Lake model mitigates the lake's excessive warming and moistening effects, weakens the convection over the downwind and mountainous regions around Lake Nam Co, and effectively reduces the over-lake T$_{2m}$ overestimation and the positive precipitation biases therein.

By adopting the model configurations in CTRL and Sen_LEC, we conduct two additional experiments running

from May 20th to November 31st 2013 to investigate the performances of the calibrated WRF-Lake during autumn, when the lake–air interactions feature strong upward vapor/heat transport due to the large positive lake–air temperature/humidity gradients and the enhanced over-lake wind speed (Wang et al. 2020). The onset (end) of lake thermal stratification is defined as the first (last) date from which the temperature differences between 6 and 56 m depths are greater than 1 °C in the subsequent (previous) 4 days without exception. The overestimated TLake$_{3m}$ during June to mid-July and the earlier onset of the lake thermal stratification in CTRL run are attributed to the unrealistically higher initial water temperature profile (Fig. 13a and b), while the underestimated TLake$_{3m}$ since mid-July and the earlier autumnal
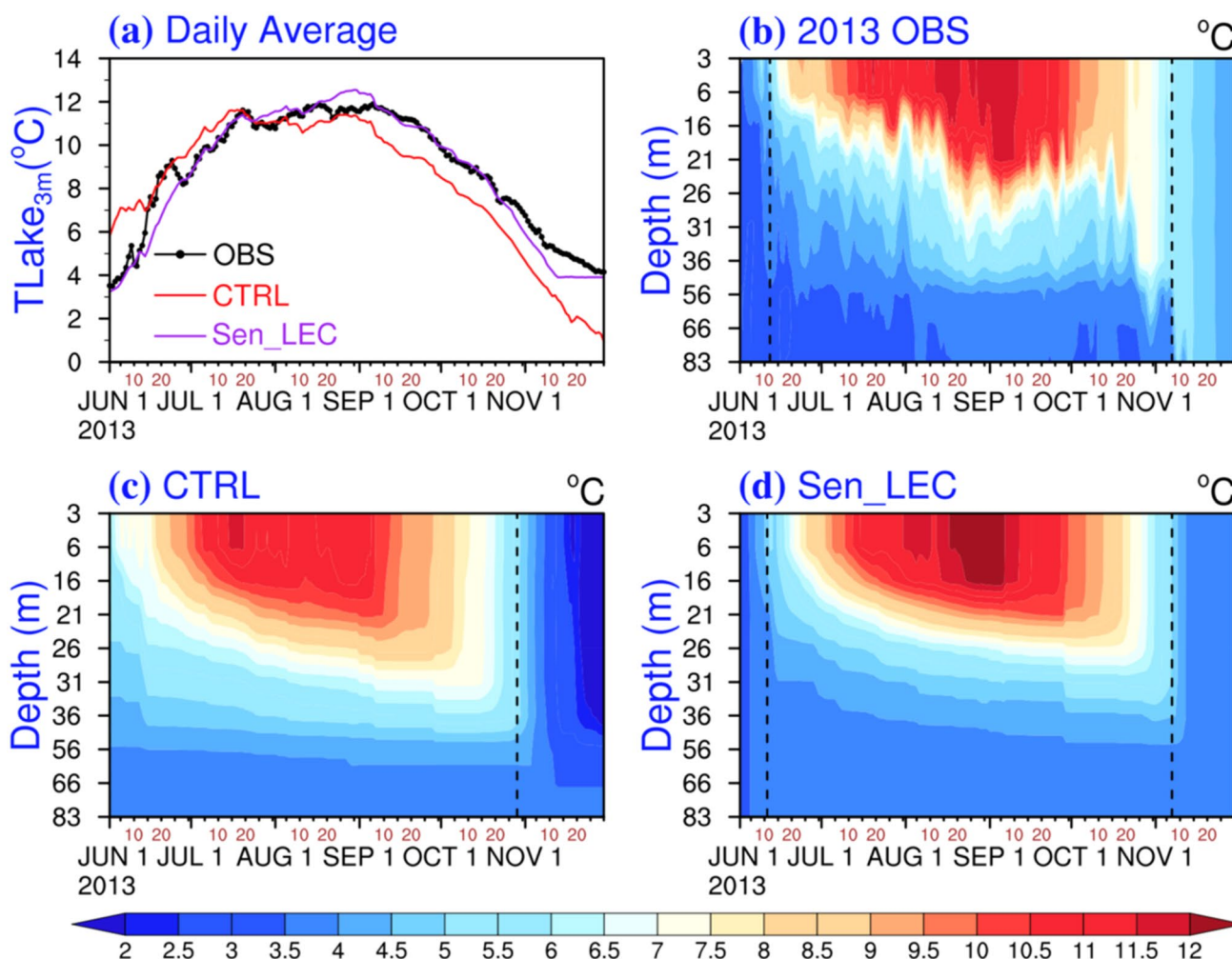
Fig. 13 a The daily TLake3m (unit: °C) from the station measurements, the CTRL and Sen_LEC simulations at the observation site during June 1st to November 30st 2013. The simultaneous time-depth distributions of the daily mean lake temperature (unit: °C) from **b** the observation, **c** CTRL, and **d** Sen_LEC simulations at the water temperature site. The black dashed lines in **b**–**d** depict the onset/end of the thermal stratification

destratification are mainly due to the excessive turbulent vapor/heat loss modulated by the large constant surface roughness length. Compared with CTRL, the Sen_LEC experiment well reproduces the surface layer lake temperature, the onset/end of thermal stratification, and the vertical water temperature variations throughout the simulation periods (Fig. 13). From Fig. 14, both CTRL and Sen_LEC generally reproduce the west–east precipitation gradient over the central TP and the westerly wind fields at 500 hPa. For the regions surrounding Lake Nam Co, the local precipitation from TRMM/ITPCAS (figure omitted) is characterized by a maximal center located to the west of the lake, namely the regions downwind the lake (marked by blue rectangle in Fig. 14f). Both experiments predict the maximal rainfall center downwind the lake despite that the precipitation intensity is overestimated. Compared with CTRL, the Sen_LEC experiment with a smaller parameterized surface roughness

length effectively restricts the upward water/heat transport and thus mitigates the rainfall overestimation downwind the lake. The 500-hPa wind field differences therein is featured by divergent patterns and the regional-averaged rainfall overestimation is reduced by 32%, from 1.18 mm·day^{-1} in CTRL to 0.8 mm·day^{-1} in Sen_LEC (Fig. 14f). The above comparisons demonstrate that the calibrated WRF-Lake is superior in modeling the autumnal lake–air interactions and the associated lake-effected regional climate surrounding the large lake basins over the central TP.

Although substantial efforts have been devoted to obtain better LST and lake–air interaction simulations, the calibrated WRF-Lake model (Sen_LEC) still exhibits disadvantages in predicting the rapid LST warming from 4.42° to 9.29 °C during June 11th–June 23th and the high-frequency oscillating variations of the metalimnion temperature (Fig. 3). These discrepancies may be attributed to both
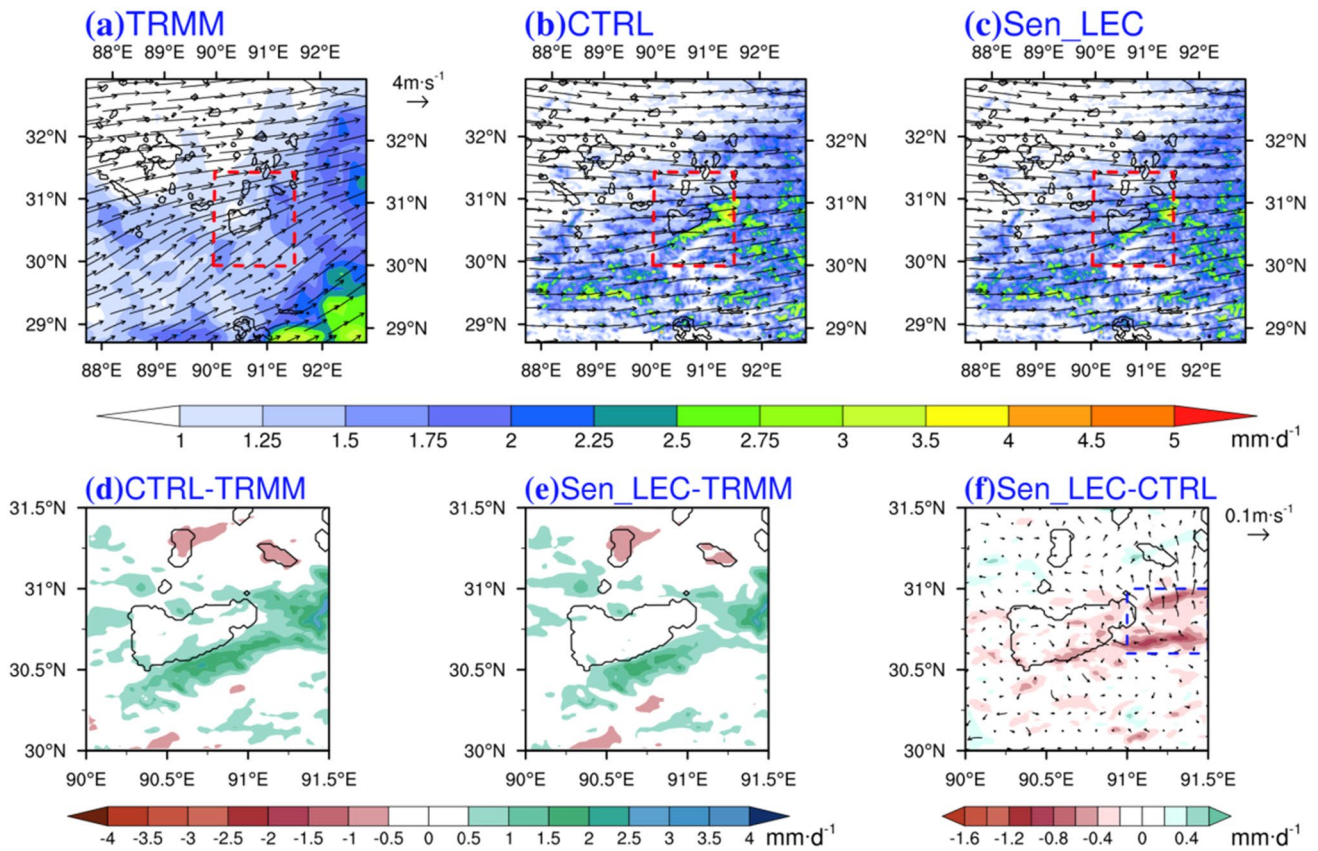
Fig. 14 Same as Fig. 9, but for the comparisons of mean rainfall and 500-hPa wind spatial distributions during autumn (September to November)

the lake model's forcing uncertainties inherited from WRF and the 1-D physical simplification by neglecting the flow-dependent heat redistribution processes within lakes. On one hand, during the rapid LST rising period in early-summer, the Sen_LEC experiment overestimates the 10-m wind speed at the Nam Co water temperature station with a maximal (mean) BIAS of 2.98 m s^{-1} (0.07 m s^{-1}), which can result in the excessive upward heat loss and therefore the underestimation of LST increase. As documented by Xu et al. (2016), the surface wind speed overestimation in WRF-Lake can be partly attributed to the smoothing orography representation over complex-terrain regions (i.e., Nyainqentanglha Mountainous area). Hence, future work needs to parameterize the unresolved turbulent orographic effects to better reproduce the surface wind speed (Jimenez et al. 2014; Zhou et al. 2019) and thus mitigate the LST underestimation. Another possible reason for the inadequate modeled LST increase at the Nam Co water temperature station is the missing heat redistribution processes related to the 3-D thermohydrodynamics. When the Lake Nam Co begins to be heated from its original thermally mixed state in early spring, LST over the shallower shore areas rises faster in response to the radiative forcing because the heat capacitiy therein is

smaller than that in the central deep lake. This would lead to the horizontal nearshore-offshore temperature gradient across the isobath (Fig. 15), which has also been reported in
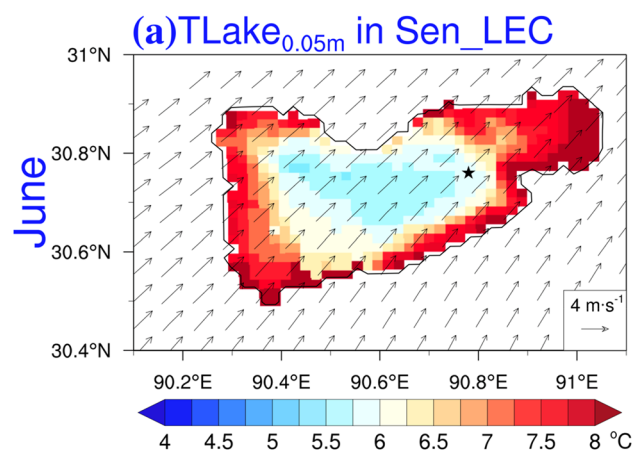
Fig. 15 The mean water temperature at 0.05 m depth (TLake$_{0.05\ m}$) from Sen_LEC over Lake Nam Co during June in 2013. The vectors are the synchronous mean wind fields at 500 hPa (unit: m s^{-1}) from ERA5 reanalysis. The black aster represents the location of the lake temperature monitoring site

Lake Victoria, Laurentian Great Lakes, and many other large deep-water bodies with sloping bottom bathymetry (Bai et al. 2013; Nyamweya et al. 2016; Rao et al. 2004). The cross-isobath temperature gradient tends to transport vast heat from the warm shore to mid-lake areas through both the horizontal temperature diffusion and the gyre-related advection induced by the baroclinic and bathymetry effects (Beletsky and Schwab 2001). In addition, accompanied by the outbreak and enhancement of the southwest monsoonal circulations (Figs. 9 and 15), the warmer epilimnetic water in the southwest shallower lake shores may experience northward advection processes and thus helps to generate the rapid LST warming at the Nam Co water temperature station. Such horizontal heat transportation processes driven by the temperature-current interactions and the prevailing surface wind have been proved to play critical roles in determining the spatiotemporal variabilities of LST over many large lakes worldwide (Song et al. 2004; Thiery et al. 2014; Xue et al. 2016). However, constrained by the 1-D structure and its simplified representation in lake mixing mechanism, WRF-Lake is unable to depict the above lake thermohydrodynamics and the rapid LST warming at deep-water Nam Co buoy since mid-June. Regarding the pronounced high-frequency oscillation of metalimnion temperature, i.e., the abrupt thermocline jump episodes during August 10th–20th, it is likely attributed to the intensive internal wave activities in the upper portion of thermocline (Huang et al. 2010; Wang et al. 2019), but the current 1-D lake scheme does not include any representation of internal waves. It remains interesting to demonstrate the benefits of employing a fully coupled 3-D lake component in the regional coupled climate models over the lake-rich TP.

References

Bai XZ, Wang J, Schwab DJ, Yang Y, Luo L, Leshkevich GA, Liu SZ (2013) Modeling 1993–2008 climatology of seasonal general circulation and thermal structure in the Great Lakes using FVCOM. Ocean Model 65:40–63. https://doi.org/10.1016/j.ocemod.2013.02.003

Balsamo G, Salgado R, Dutra E, Boussetta S, Stockdale T, Potes M (2012) On the contribution of lakes in predicting near-surface temperature in a global weather forecasting model. Tellus A: Dyn Meteorol Oceanogr. https://doi.org/10.3402/tellusa.v64i0.15829

Beletsky D, Schwab DJ (2001) Modelling circulation and thermal structures in Lake Michigan: annual cycle and interannual variability. J Geophys Res 106:745–771. https://doi.org/10.1029/2000JC000691

Biermann T, Babel W, Ma WQ, Chen XL, Thiem E, Ma YM, Foken T (2014) Turbulent flux observations and modelling over a shallow lake and a wet grassland in the Nam Co basin, Tibetan Plateau. Theor Appl Climatol 116:301–316. https://doi.org/10.1007/s00704-013-0953-6

Chen TA, Millero FJ (1986) Precise thermodynamic properties for natural waters covering only the limnological range. Limnol Oceanogr 31(3):657–662. https://doi.org/10.4319/lo.1986.31.3.0657

Chen YY, Yang K, He J, Qin J, Shi JC, Du JY, He Q (2011) Improving land surface temperature modeling for dry land of China. J Geophys Res 116:D20104. https://doi.org/10.1029/2011JD015921

Choulga M, Kourzeneva E, Zakharova E, Doganovsky A (2014) Estimation of the mean depth of boreal lakes for use in numerical weather prediction and climate modelling. Tellus A. https://doi.org/10.3402/tellusa.v66.21295

Dai A, Trenberth KE (2004) The diurnal cycle and its depiction in the community climate system model. J Clim 17:930–951. https://doi.org/10.1175/1520-0442(2004)017<0930:TDCAID>2.0.CO;2

Dai YF, Wang L, Yao TD, Li XY, Zhu LJ, Zhang XW (2018a) Observed and simulated lake effect precipitation over the Tibetan Plateau: an initial study at Nam Co Lake. J Geophys Res Atmos 123:6746–6759. https://doi.org/10.1029/2018JD028330

Dai YF, Yao TD, Li XY, Ping F (2018b) The impact of lake effects on the temporal and spatial distribution of precipitation in the Nam Co basin, Tibetan Plateau. Quatern Int 475:63–69. https://doi.org/10.1016/j.quaint.2016.01.075

Dai YJ, Wei N, Huang AN, Zhu SG, Shang W, Yuan H, Zhang SP, Liu SF (2018c) The lake scheme of the common land model and its performance evaluation. Chin Sci Bull 63(28–29):3002–3021. https://doi.org/10.1360/N972018-00609

Dudhia J (1989) Numerical study of convection observed during the winter monsoon experiment using a mesoscale two-dimensional model. J Atmos Sci 46:3077–3107. https://doi.org/10.1175/1520-0469(1989)046<3077:NSOCOD>2.0.CO;2

Friedl MA, Sulla-Menashe D, Tan B, Scheneider A, Ramankutty N, Sibley A, Huang XL (2010) MODIS collection 5 global land cover: algorithm refinements and characterization of new datasets. Remote Sens Environ 114:168–182. https://doi.org/10.1016/j.rse.2009.08.016

Gerken T, Biermann T, Babel W, Herzog M, Ma YM, Foken T, Graf HF (2013) A modelling investigation into lake–breeze development and convection triggering in the Nam Co Lake basin, Tibetan Plateau. Theor Appl Climatol 117(1–2):149–167. https://doi.org/10.1007/s00704-013-0987-9

Goyette S, McFarlane NA, Flato GM (2000) Application of the Canadian regional climate model to the Laurentian great lakes region: implementation of a lake model. Atmos Ocean 38(3):481–503. https://doi.org/10.1080/07055900.2000.9649657

Grell GA, Devenyi D (2002) A generalized approach to parameterizing convection combining ensemble and data assimilation techniques. Geophys Res Lett 29(14):1693. https://doi.org/10.1029/2002GL015311

Gu HP, Jin JM, Wu YH, Ek MB, Subin ZM (2015) Calibration and validation of lake surface temperature simulations with the coupled WRF-lake model. Clim Change 129:471–483. https://doi.org/10.1007/s10584-013-0978-y

Gu HP, Ma ZG, Li MX (2016) Effect of a large and very shallow lake on local summer precipitation over the Lake Taihu basin in China. J Geophys Res Atmos 121:8832–8848. https://doi.org/10.1002/2015JD024098

Guo YH, Zhang YS, Ma N, Xu JQ, Zhang T (2019) Long-term changes in evaporation over Siling Co Lake on the Tibetan Plateau and its impact on recent rapid lake expansion. Atmos Res 216:141–150. https://doi.org/10.1016/j.atmosres.2018.10.006

Hakanson L (1995) Models to predict Secchi depth in small glacial lakes. Aquat Sci 57:31–53. https://doi.org/10.1007/BF00878025

He J, Yang K, Tang WJ, Lu H, Qin J, Chen YY, Li X (2020) Data descriptor: The first high-resolution meteorological forcing dataset for land process studies over China. Sci Data 7(25):1–11. https://doi.org/10.1038/s41597-020-0369-y

Hong SY, Lim J (2006) The WRF single-moment 6-class microphysics scheme (WSM6). J Korean Meteorol Soc 42:129–151

Hong SY, Noh Y, Dudhia J (2006) A new vertical diffusion package with an explicit treatment of entrainment processes. Mon Wea Rev 134:2318–2341. https://doi.org/10.1175/MWR3199.1

Hook SJ, Prata FJ, Alley RE, Abtahi A, Richards RC, Schladow SG, Pálmarsson S (2003) Retrieval of Lake Bulk and skin temperatures using along-track scanning radiometer (ATSR-2) data: a case study using Lake Tahoe, California. J Atmos Ocean Technol 20:534–548. https://doi.org/10.1175/1520-0426(2003)20<534:ROLBAS>2.0.CO;2

Hostetler SW, Bates GT, Giorgi F (1993) Interactive coupling of a lake thermal model with a regional climate model. J Geophys Res 98:5045–5057. https://doi.org/10.1029/92JD02843

Huang AN, Rao YR, Lu YY (2010) Evaluation of a 3-D hydrodynamic model and atmospheric forecast forcing using observations in Lake Ontario. J Geophys Res 115:C02004. https://doi.org/10.1029/2009JC005601

Huang L, Wang JB, Zhu LP, Ju JT, Daut G (2017) The warming of large lakes on the Tibetan Plateau: evidence from a lake model simulation of Nam Co, China, during 1979–2012. J Geophys Res 122:13095–13107. https://doi.org/10.1002/2017JD027379

Huang AN, Wang JB, Dai YJ, Yang K, Wei N, Wen LJ, Wu Y, Zhu XY, Zhang XD, Cai SX (2019) Evaluating and improving the performance of three 1-D Lake models in a large deep lake of the Central Tibetan Plateau. J Geophys Res. https://doi.org/10.1029/2018JD029610

Huffman GJ, Bolvin DT, Nelkin EJ, Wolff DB, Adler RF, Gu G, Hong Y, Bowman KP, Stocker EF (2007) The TRMM multisatellite precipitation analysis (TMPA): quasi-global, multiyear, combined-sensor precipitation estimates at fine scales. J Hydrometeor 8:38–55. https://doi.org/10.1175/JHM560.1

Hwang C, Cheng YS, Yang WH et al (2019) Lake level changes in the Tibetan Plateau from Cryosat-2, SARAL, ICESat, and Jason-2 atimeters. Terr Atmos Ocean Sci 30:1–18. https://doi.org/10.3319/TAO.2018.07.09.01

Imberger J, Patterson JC (1981) A dynamic reservoir simulation model—DYRESM: 5. Transport Models/Inland Coast Waters. https://doi.org/10.1016/b978-0-12-258152-6.50014-2

Jiang JH, Huang Q (2004) Distribution and variation of lakes in Tibetan Plateau and their comparison with lakes in other parts of China. Water Resour Protect 15(6):24–28

Jiang LG, Karina N, Andersen OB, Gottwein PB (2017) Monitoring recent lake level variations on the Tibetan Plateau using CryoSat-2 SARIn mode data. J Hydro 544:109–124. https://doi.org/10.1016/j.jhydrol.2016.11.024

Jimenez P, de Arellano JV, Navarro J, Gonzalez-Rouco JF (2014) Understanding land–atmosphere interactions across a range of spatial and temporal scales. Bull Am Meteor Soc 95:ES14–ES17. https://doi.org/10.1175/BAMS-D-13-00029.1

Karl H, Jeppesen E (2018) Ecological responses of lakes to climate change. Water 2018(10):917. https://doi.org/10.3390/w10070917

Kleinherebrink M, Lindenbergh RC, Ditmar PG (2015) Monitoring of lake level changes on the Tibetan Plateau and Tian Shan by retracking Cryosat SARIn waveforms. J Hydro 521:119–131. https://doi.org/10.1016/j.jhydrol.2014.11.063

Kourzeneva E (2010) External data for lake parameterization in numerical weather prediction and climate modeling. Boreal Environ Res 15:165–177

Kourzeneva E, Asensio H, Martin E, Faroux S (2012) Global gridded dataset of lake coverage and lake depth for use in numerical weather prediction and climate modelling. Tellus A 64:15640. https://doi.org/10.3402/tellusa.v64i0.15640

Lang JH, Lyu SH, Li ZG, Ma YM, Su DS (2018) An investigation of ice surface albedo and its influence on the of high-altitude lakes the Tibetan Plateau. Remote Sens 10:218. https://doi.org/10.3390/rs10020218

Lazhu KY, Wang JB, Lei YB, Chen YY, Zhu LP, Ding BH, Qin J (2016) Quantifying evaporation and its decadal change for Lake Nam Co, central Tibetan Plateau. J Geophys Res 121:7578–7591. https://doi.org/10.1002/2015JD024523

Li ZG, Lv SH, Ao YH, Wen LJ, Zhao L, Wang SY (2015) Long-term energy flux and radiation balance observations over Lake Ngoring, Tibetan Plateau. Atmos Res 155:13–25. https://doi.org/10.1016/j.atmosres.2014.11.019

Li ZG, Ao YH, Lv SH, Lang JH, Wen LJ, Stepanenko V, Meng XH, Zhao L (2018) Investigation of the ice surface albedo in the Tibetan Plateau lakes based on the field observation and MODIS products. J Glaciol. https://doi.org/10.1017/jog.2018.35

Liao JJ, Shen GZ, Li YK (2013) Lake variations in response to climate change in the Tibetan Plateau in the past 40 years. Int J Digit Earth. https://doi.org/10.1080/17538947.2012.656290

Lofgren BM (1997) Simulated effects of idealized Laurentian Great Lakes on regional and large-scale climate. J Climate 10:2847–2858. https://doi.org/10.1175/1520-0442(1997)010<2847:SEOILG>2.0.CO;2

Ma RH, Yang GS, Duan HT, Jiang JH, Wang SM, Feng XZ, Li AN, Kong FX, Xue B, Wu JL, Lin SJ (2011) China's lakes at present: number, area and spatial distribution. Sci China Earth Sci 54:283–289. https://doi.org/10.1007/s11430-010-4052-6

Ma YM, Han CB, Zhong L, Wang BB, Zhu ZK, Wang YJ, Zhang L, Meng CC, Xu C, Amatya PM (2014) Using MODIS and AVHRR data to determine regional surface heating field and heat flux distributions over the heterogeneous landscape of the Tibetan Plateau. Theor Appl Climatol 117:643–652. https://doi.org/10.1007/s00704-013-1035-5

Mallard MS, Nolte CG, Bullock OR, Spero TL, Gula J (2014) Using a coupled lake model with WRF for dynamical downscaling. J Geophys Res 119:7193–7208. https://doi.org/10.1002/2014JD021785

Martynov A, Sushama L, Laprise R, Winger K, Dugas B (2012) Interactive lakes in the Canadian regional climate model, version 5: The role of lakes in the regional climate of North America. Tellus 64A:16226. https://doi.org/10.3402/tellusa.v64i0.16226

Martynov A, Laprise R, Sushama L, Winger K, Separovic L, Dugas B (2013) Reanalysis-driven climate simulation over CORDEX North America domain using the Canadian Regional Climate Model, version 5: model performance evaluation. Clim Dyn 41:2973. https://doi.org/10.1007/s00382-013-1778-9

Maussion F, Scherer D, Molg T, Collier E, Curio J, Finkelnburg R (2013) Precipitation seasonality and variability over the Tibetan Plateau as resolved by the high Asia reanalysis. J Climate 27:1910–1927. https://doi.org/10.1175/JCLI-D-13-00282.1

Mironov DV (2008) Parameterization of lakes in numerical weather prediction. Description of a lake model [R]. COSMO technical report. Deutscher Wetterdienst, Offenbach am Main, Germany.

Mironov DV, Heise E, Kourzeneva E, Ritter B, Scgneider N, Terzhevik A (2010) Implementation of the lake parameterisation scheme FLake into the numerical weather prediction model COSMO. Boreal Environ Res 15:218–230

Mitchell K, Mike EK, Vince W, Dag L, Paul R (2005) The community Noah land–surface model (LSM).

Mlawer EJ, Taubman SJ, Brown PD, Iacono MJ, Clough SA (1997) Radiative transfer for inhomogeneous atmospheres: RRTM, a validated correlated-k model for the longwave. J Geophys Res 102(D14):16663–16682. https://doi.org/10.1029/97JD00237

Neckel N, Kropacek J, Bolch T, Hochschild V (2014) Glacier mass changes on the Tibetan Plateau 2003–2009 derived from ICE-Sat laser altimetry measurements. Environ Res Lett 9(1):1–7. https://doi.org/10.1088/1748-9326/9/1/014009

Notaro M, Holman K, Zarrin A, Fluck E, Vavrus S, Bennington V (2013) Influence of the Laurentian Great Lakes on regional climate. J Clim 26:789–804. https://doi.org/10.1175/JCLI-D-12-00140.1

Nyamweya C, Desjardins C, Sigurdsson S, Tomasson T, Munyaho AT, Sitoki L, Stefansson G (2016) Simulation of Lake Victoria circulation patterns using the regional ocean modeling system (ROMS). PLoS ONE 11(3):e0151272. https://doi.org/10.1371/journal.pone.0151272

Oleson K et al (2004) Technical description of the community land model (CLM). NCAR Technical Note NCAR/TN-461+STR. Doi: https://doi.org/10.5065/D6N877R0

Pan H, Avissar R, Haidvogel DB (2002) Summer circulation and temperature structure of Lake Kinneret. J Phys Oceanogr 32(1):295–313. https://doi.org/10.1175/1520-0485(2002)032<0295:SCATSO>2.0.CO;2

Perroud M, Goyette S, Martynov A, Beniston M, Anneville O (2009) Simulation of multiannual thermal profiles in deep Lake Geneva: a comparison of one-dimensional lake models. Limnol Oceanogr 54(5):1574–1594. https://doi.org/10.4319/lo.2009.54.5.1574

Qi MM, Yao XJ, Li XF, Duan HY, Gao YP, Liu J (2019) Spatiotemporal characteristics of Qinghai Lake ice phenology between 2000 and 2016. J Geogr Sci 29(1):115–130. https://doi.org/10.1007/s11442-019-1587-0

Rao YR, Skafel MG, Charlton MN (2004) Circulation and turbulent exchange characteristics during the thermal bar in Lake Ontario. Limnol Oceanor 49(6):2190–2200. https://doi.org/10.4319/lo.2004.49.6.2190

Sahoo GB, Forrest AL, Schladow SG, Reuter JE, Coats R, Dettinger MD (2016) Climate change impacts on lake thermal dynamics and ecosystem vulnerabilities. Limnol Oceanogr 61:496–507. https://doi.org/10.1002/lno.10228

Samuelsson P, Kourzeneva E, Mironov D (2010) The impact of lakes on the European climate as simulated by a regional climate model. Boreal Environ Res 15(2):113–129

Sharma A, Hamlet AF, Fernando HJS, Catlett CE, Horton DE, Kotamarthi VR, Kristovich DAR, Packman AI, Tank JL, Wuebbles DJ (2018) The need for an integrated land-lake–atmosphere modeling system, exemplified by North America's Great Lakes region. Earth's Future 6:1366–1379. https://doi.org/10.1029/2018EF000870

Simmons AS, Uppala S, Dee D, Kobayashi S (2007) ERA-Interim: New ECMWF reanalysis products from 1989 onwards. ECMWF Newslett 110:25–35. https://doi.org/10.21957/pocnex23c6

Skamarock WC, Klemp JB, Dudhia J, Gill DO, Barker DM, Duda MG, Huang XY, Wang W, Powers JG (2008) A description of the advanced research WRF version 3. NCAR Technical Note NCAR/TN-475+STR. Doi: https://doi.org/10.5065/D68S4MVH

Song Y, Semazzi FHM, Xie L, Ogallo LJ (2004) A coupled regional climate model for the Lake Victoria basin of East Africa. Int J Climatol 24:57–75. https://doi.org/10.1002/joc.983

Song CQ, Huang B, Ke LH (2013) Modeling and analysis of lake water storage changes on the Tibetan Plateau using multi-mission satellite data. Remote Sens Environ 135:25–35. https://doi.org/10.1016/j.rse.2013.03.013

Song KS, Wang M, Du J, Yuan Y, Ma JH, Mu GY (2016) Spatiotemporal variations of lake surface temperature across the Tibetan Plateau using MODIS LST product. Remote Sens 8:854. https://doi.org/10.3390/rs8100854

Stepanenko VM, Goyette S, Martynov A, Perroud M, Fang X, Mironov D (2010) First steps of a lake model intercomparison project: LakeMIP. Boreal Environ Res 15:191–202

Stepanenko VM, Martynov A, Johnk KD, Subin ZM, Perround M, Fang X, Beyrich F, Mironov D, Goyette S (2013) A one-dimensional model intercomparison study of thermal regime of a shallow, turbid midlatitude lake. Geosci Model Dev 6:1337–1352. https://doi.org/10.5194/gmd-6-1337-2013

Subin ZM, Riley WJ, Mironov D (2012) An improved lake model for climate simulations: model structure, evaluation, and sensitivity analyses in CESM1. J Adv Model Earth Syst 4:M02001. https://doi.org/10.1029/2011MS000072

Taylor KE (2001) Summarizing multiple aspects of model performance in a single diagram. J Geophys Res Atoms 106:7183–7192. https://doi.org/10.1029/2000JD900719

Theeuwes NE, Steeneveld GJ, Krikken F, Holtslag AAM (2010) Mesoscale modeling of lake effect snow over Lake Erie—Sensitivity to convection, microphysics and the water temperature. Adv Sci Res 4:15–22. https://doi.org/10.5194/asr-4-15-2010

Thiebaux J, Rogers E, Wang WQ, Katz B (2003) A new high-resolution blended real-time global sea surface temperature analysis. Bull Amer Meteor Soc 84:645–656. https://doi.org/10.1175/BAMS-84-5-645

Thiery W, Martynov A, Darchambeau F, Descy JP, Plisnie PD, Sushama L, Lipzig NPM (2014) Understanding the performance of the FLake model over two African Great Lakes. Geosci Model Dev 7:317–337. https://doi.org/10.5194/gmd-7-317-2014

Thiery W, Davin EL, Panitz HJ, Demuzere M, Lhermitte S, Lipzig NV (2015) The impact of the African Great Lakes on the regional climate. J Clim 28:4061–4085. https://doi.org/10.1175/JCLI-D-14-00565.1

Wan Z, Zhang Y, Zhang Q, Li ZL (2004) Quality assessment and validation of the MODIS global land surface temperature. Int J Remote Sens 25:261–274. https://doi.org/10.1080/0143116031000116417

Wang JB, Zhu LP, Daut G, Ju JT, Lin X, Wang Y, Zhen XL (2009) Investigation of bathymetry and water quality of Lake Nam Co, the largest lake on the central Tibetan Plateau. Limnology 10:149–158. https://doi.org/10.1007/s10201-009-0266-8

Wang BB, Ma YM, Chen XL, Ma WQ, Su ZB, Menenti M (2015) Observation and simulation of lake–air heat and water transfer processes in a high-altitude shallow lake on the Tibetan Plateau. J Geophys Res Atmos 120:12327–12344. https://doi.org/10.1002/2015JD023863

Wang BB, Ma YM, Ma WQ, Su ZB (2017) Physical controls on half-hourly, daily, and monthly turbulent flux and energy budget over a high-altitude small lake on the Tibetan Plateau. J Geophys Res 122:2289–2303. https://doi.org/10.1002/2016JD026109

Wang FS, Ni GH, Riley WJ, Tang JY, Zhu DJ, Sun T (2018) Evaluation of the WRF lake module (v1.0) and its improvements at a deep

reservoir. Geosci Model Dev Discuss. https://doi.org/10.5194/gmd-2018-168

Wang JB, Huang L, Ju JT, Daut G, Wang Y, Ma QF, Zhu LP, Haberzettl T, Baade J, Mausbacher R (2019) Spatial and temporal variations in water temperature in a high-altitude deep dimictic mountain lake (Nam Co), central Tibetan Plateau. J Great Lakes Res. https://doi.org/10.1016/j.jglr.2018.12.005

Wang JB, Huang L, Ju JT, Laval BE (2020) Seasonal stratification of a deep, high-altitude, dimictic lake: Nam Co, Tibetan Plateau. J Hydrol. https://doi.org/10.1016/j.jhdyrol.2020.124668

Wen LJ, Lv SH, Li ZG, Zhao L, Nagabhatla N (2015) Impact of two biggest lakes on local temperature and precipitation in the Yellow River source region of the Tibetan Plateau. Adv Meteorol. https://doi.org/10.1155/2015/248031

Wen LJ, Lv SH, Kirillin G, Li ZG, Zhao L (2016) Air–lake boundary layer and performance of a simple lake parameterization scheme over the Tibetan highlands. Tellus A: Dyn Meteorol Oceanogr 68(1):31091. https://doi.org/10.3402/tellusa.v68.31091

Williams K, Chamberlain J, Buontempo C, Bain C (2015) Regional climate model performance in the Lake Victoria basin. Climate Dyn 44:1699–1713. https://doi.org/10.1007/s00382-014-2201-x

Wu Y, Huang AN, Yang B, Dong GT, Wen LJ, Lazhu ZQZ, Fu ZP, Zhu XY, Zhang XD, Cai SX (2019) Numerical study on the climatic effect of the lake clusters over Tibetan Plateau in summer. Climate Dyn. https://doi.org/10.1007/s00382-019-04856-4

Xiao CL, Lofgren BM, Wang J, Chu PY (2016) Improving the lake scheme within a coupled WRF-lake model in the Laurentian Great Lakes. J Adv Model Earth Syst 8:1969–1985. https://doi.org/10.1002/2016MS000717

Xiao CL, Lofgren BM, Wang J, Chu PY (2018) A dynamical downscaling projection of future climate change in the Laurentian Great Lakes region using a coupled air-lake model. Preprints. https://doi.org/10.20944/preprints201807.0468.v1

Xu LJ, Liu HZ, Du Q, Wang L (2016) Evaluation of the WRF-lake model over a highland freshwater in southwest China. J Geophys Res. https://doi.org/10.1002/2016JD025396

Xu LJ, Liu HZ, Du Q, Wang L, Yang L, Sun JH (2019) Differences of atmospheric boundary layer characteristics between pre-monsoon and monsoon period over the Erhai Lake. Theor Appl Climatol 135:305. https://doi.org/10.1007/s00704-018-2386-8

Xue PF, Pal JS, Ye XY, Lenters JD, Huang CF, Chu PY (2016) Improving the simulation of large lakes in regional climate modeling: two-way lake–atmosphere coupling with a 3D hydrodynamic

model of the Great Lakes. J Clim. https://doi.org/10.1175/JCLI-D-16-0225.1

Yan FQ, Sillanpaa M, Kang SC, Aho KS, Qu B, Wei D, Li XF, Li CL, Raymond PA (2018) Lakes on the Tibetan Plateau as conduits of greenhouse gases to the atmosphere. J Geophys Res. https://doi.org/10.1029/2017JG004379

Yang B, Zhou Y, Zhang YC, Huang AN, Qian Y, Zhang LJ (2017) Simulated precipitation diurnal cycles over East Asia using different CAPE-based convective schemes in WRF model. Clim Dyn 50:1639–2165. https://doi.org/10.1007/s00382-017-3712-z

Zhang X, Duan KQ, Shi PH, Yang JH (2016) Effect of lake surface temperature on the summer precipitation over the Tibetan Plateau. J Mt Sci 13(5):802–810. https://doi.org/10.1007/s11629-015-3743-z

Zhang GQ, Yao TD, Piao SL, Bolch T, Xie HJ, Chen DL, Gao YH, O'Reilly CM, Shum CK, Yang K, Shuang Y, Lei YB, Wang WC, He Y, Shang K, Yang XK, Zhang HB (2017) Extensive and drastically different alpine lake changes on Asia's high plateaus during the past four decades. Geophys Res Lett 44:252–260. https://doi.org/10.1002/2016GL072033

Zhang GQ, Luo W, Chen W, Zheng G (2019a) A robust but variable lake expansion on the Tibetan Plateau. Sci Bull 64(18):1306–1309. https://doi.org/10.1016/j.scib.2019.07.018

Zhang QH, Jin JM, Wang XC, Budy P, Barrett N, Null SE (2019b) Improving lake mixing process simulations in the community land model by using K profile parameterization. Hydrol Earth Syst Sci 23(12):4969–4982. https://doi.org/10.5194/hess-23-4969-2019

Zhou X, Yang K, Beljaars A, Li HD, Lin CG, Huang B, Wang Y (2019) Dynamical impact of parameterized turbulent orographic form drag on the simulation of winter precipitation over the western Tibetan Plateau. Clim Dyn 53:707–720. https://doi.org/10.1007/s00382-019-04628-0

Zhu LJ, Jin JM, Liu X, Tian L, Zhang QH (2017) Simulations of the impact of lakes on local and regional climate over the Tibetan Plateau. Atmos Ocean. https://doi.org/10.1080/07055900.2017.1401-524

Publisher's Note Springer Nature remains neutral with regard to jurisdictional claims in published maps and institutional affiliations.